5-18-2007

Highly Ordered Hexagonal Mesoporous Silica as Hosts and Templates for Encapsulation of Germanium Semiconductor Clusters

Yi Wang
University of New Orleans

Highly Ordered Hexagonal Mesoporous Silica as Hosts and Templates for Encapsulation of Germanium Semiconductor Clusters

A Thesis

Submitted to the Graduate Faculty of the
University of New Orleans
in Partial fulfillment of the
requirements for the degree of

Master of Science
In
The Department of Chemistry

By

Yi Wang

B.S, University of Science and Technology of China, 1998

May, 2007

ACKNOWLEDGEMENTS

I would like to thank especially my supervisor, Dr. Jiye Fang, for his inspiration, guidance and encouragement throughout the duration of this research work. His ideas and advices have been decisive to improve this thesis.

I would like to acknowledge Dr. Heike Gabrisch and Dr. Kevin Stokes who agreed to be on my committee for their help and insight they gave to me throughout this research.

I would also like to thank Dr. Qiang Cai, who worked and generously shared his experience and suggestions with me.

Lastly, and most importantly, I wish to thank my parents, Zuojun Wang and Yuhua Zhou, for their efforts and for being there for me. To them I dedicate this thesis.

TABLE OF CONTENTS

LIST OF FIGURES vi
ABSTRACT viii

CHAPTER 1: INTRODUCTION 1

1.1 Background of Mesoporous Materials 1
1.1.1 Surfactant Templates 2
1.1.2 Formation Mechanism 3
1.1.3 Thermodynamics 6
1.2 Sol-gel synthesis of ordered mesoporous oxides 8
1.3 Encapsulation of Germanium semiconductor clusters 9
1.4 Scope and Objectives 9

CHAPTER 2: EXPERIMENTAL 11

2.1 Chemical Reagents 11
2.2 Synthesis Techniques 11
2.2.1 General Techniques to synthesis MCM-41 11
2.2.2 Encapsulation of Ge nanoparticles into MCM-41 12
2.3 Analysis and Characterization 14
2.3.1 X-ray Powder diffraction (XRD) 14
2.3.2 Transmission Electron Microscopy (TEM) 14
2.3.3 Energy Dispersive Spectroscopy (EDS) 14
2.3.4 Scanning Electron Microscope (SEM) 15
2.3.5 N_2 absorption and desorption 15

CHAPTER 3: PREPARATION OF THE MESOPOROUS SILICA WITH VARIOUS MORPHOLOGIES 16

3.1 Synthesis of micrometer-sized MCM-41 particles 17

3.1.1 Synthesis conditions 17

3.1.2 Results and discussions 17

3.2 Synthesis of large monolith MCM-41 rod 21

3.2.1 Synthesis conditions 21

3.2.2 Results and discussions 21

3.3 Synthesis of MCM-41 film 25

3.3.1 Synthesis conditions 25

3.3.2 Results and discussions 26

3.4 Synthesis of uniform rice-like MCM-41 particles 28

3.4.1 Synthesis conditions 28

3.4.2 Results and discussions 30

3.5 Synthesis of helical MCM-41 silica 30

3.5.1 Synthesis conditions 30

3.5.2 Results and discussions 30

3.6 Summary 30

CHAPTER 4: ENCAPSULATION OF GEMANIUM NANOPARTICLES INSIDE MCM-41 MESOPORES 33

4.1 H_2 reduction method 33

4.1.1 Experiment method 33

4.1.2 Electron Microscope results 34

4.1.3 XRD results 38

4.1.4 EDS analysis 38

4.1.5 N_2 adsorption-desorption study 39

4.2 Vapor phase epitaxy 41

4.2.1 Experiment method 41

4.2.2 Results and analysis 41

4.3 Redox reaction using Na-Naphthalene 42
4.3.1 Experiment method 42
4.3.2 Results and analysis 43
4.4 Summary 44

CHAPTER 5: CONLUSIONS 45

REFERENCES 47

VITA 50

LIST OF FIGURES

Figure 1.1 The phase diagram of cationic surfactant CTAB in aqueous solution 2

Figure 1.2 Schematic model of liquid crystal templating mechanism via two possible pathways 4

Figure 1.3 Schematic model for transformation mechanism from lamellar to hexagonal phase ... 5

Figure 1.4 Schematic representation of the different types of silica-surfactant interfaces 6

Figure 1.5 The interrelationship between solvent, template and inorganic species 7

Figure 3.1 SEM images of ordered MCM-41 particles: A) Scale bar, 2 μm. B) Scale bar, 500 nm 19

Figure 3.2 TEM images of ordered MCM-41 particles: A) Scale bar, 500 nm. B) Scale bar, 20 nm. C) Scale bar, 100 nm. D) Scale bar, 20 nm) 20

Figure 3.3 SEM images of rod-like MCM-41 from the 1st time of seed crystal growth..... 22

Figure 3.4 SEM images of rod-like MCM-41 from the 2nd time of seed crystal growth 23

Figure 3.5 SEM images of MCM-41 rod from the 3rd time of seed crystal growth 24

Figure 3.6 SEM images of MCM-41 thin film. A) the sample was collected directly from the synthesis solution. B) the sample was collected after filtration 26

Figure 3.7 SEM images of MCM-41 films with thickness of about 300 nm: A) Scale bar, 4 μm. B) Scale bar, 4 μm. C) Films immersed in the solution. D) Films dispersed in ethanol 27

Figure 3.8 Graphical illustration of the proposed mechanism for the formation of mesoporous silica film at the air-water interface [63]..... 28

Figure 3.9 SEM images of rice-like MCM-41 particles 29

Figure 3.10 SEM images of helical MCM-41 31

Figure 4.1 schematic reaction sequences for the synthesis of Ge nanoparticles in MCM-41 34

Figure 4.2 TEM images of Ge@MCM-41 sample 1: A) TEM image of Ge@MCM-41 composite particles. B) High magnification of a single Ge@MCM-41 particle. C) Electron diffraction pattern of Ge@MCM-41 composite particle viewing along the axis of hexagonal pores. D) One-

dimensional electron diffraction pattern of Ge@MCM-41 obtained by viewing normal to the hexagonal pore axis 35

Figure 4.3 TEM images of Ge@MCM-41 sample 2: A) Scale bar, 200 nm. B) Scale bar, 100 nm 36

Figure 4.4 TEM images of Ge@MCM-41 sample 3: A) Scale bar, 500 nm. B) Scale bar, 100 nm 36

Figure 4.5 SEM images of sample 3: A) Scale bar, 2 um. B) Scale bar, 500 nm 37

Figure 4.6 A) Low-angle (2θ=1-10o) XRD pattern of empty MCM-41 and loaded Ge@MCM-41. B) Wide-angle (2θ=10-80o) XRD pattern of loaded Ge@MCM-41 37

Figure 4.7 EDS patterns of three samples through H2 reduction synthesis route: A) Sample 1 via single impregnation. B) Sample 2 via multiple impregnations. C) Sample 3 via multiple impregnations and after calcinations 39

Figure 4.8 Nitrogen adsorption-desorption isotherms of (a) Empty MCM-41 and (b) Ge@MCM-41 40

Figure 4.9 TEM images of Ge@MCM-41 synthesize through Vapor phase epitaxy method 42

Figure 4.10 EDS pattern of Ge@MCM-41 composites synthesized through Na-Naphthalene reduction 43

Figure 4.11 TEM images of Ge@MCM-41 synthesized through Na-Naphthalene reduction 43

ABSTRACT

Highly ordered mesoporous MCM-41 silica particles with several morphologies have been synthesized in an alkaline solution using cationic amphiphilic surfactant CTAB as template. The size and the morphology were controlled by varying the reaction temperature and time or by controlling the crystallization process of silica. The characterization results showed that highly ordered mesoporous particles were obtained, which had smooth surface, controllable size and high thermal stability.

Germanium semiconductor clusters were encapsulated into hexagonal MCM-41 nanoparticles with a uniform pore size around 500nm via three different synthesis routes (H_2 reduction, Vapor phase epitaxy and Na-Naphthalene reduction). Crucial parameters and experimental skills were discovered for reproducibly preparation in each system. It is found that H_2 reduction method can effectively load Ge nanoparticles into the pores of MCM41. A series of experiments were performed in the system for a more thorough understanding of the synthesis process.

CHAPTER 1 INTRODUCTION

1.1. Background of Mesoporous Materials

In the process of development of nanomaterials, the long-range ordered porous materials have attracted much attention because of their unique structures and properties. According to IUPAC nomenclature [1], porous solid can be classified, depending on their pore size (diameter, *d*), into three categories, viz., microporous (d < 2nm), mesoporous (2nm < d < 50nm), and macroporous (d > 50nm). Porous materials have huge surface areas, providing a vast number of sites where sorption processes can occur. These materials have numerous applications in catalysis, separation and many other fields [2-6]. The synthesis of these materials is of considerable interest and is constantly being developed to introduce different properties.

New mesoporous organized silicates have been synthesized using a templating technique of which the MCM-41 (Mobile Crystalline Material) [7] is typical. It is ordered to some degree and exhibits a two-dimensional hexagonal arrangement of uniform mesopores. The walls of the channels are amorphous SiO_2. The new concept in the synthesis strategy of these porous composite materials is the adoption of a self-assembled molecular aggregate or supramolecular assembly of surfactant molecules. The self-assembled microstructure serves as structure-directing agents. The hexagonal arranged MCM-41, together with MCM-48 which has a cubic structure with a three-dimensional pore system, and two other thermally unstable phases (lamellar and octamer), belong to the M41S family [7-8].

A lot of progresses have been made based on the fundamental work of Mobil researchers, such as other silica-based mesophases (e.g. FSM-16 [9], SBA-15 [10], and MSU-1 [11]) and non-silica-based mesophases (e.g. Aluminophosphates [12] and carbons [13]). These mesoporous materials are of great importance in diverse areas, such as catalysis, adsorption, and guest-host chemistry.

1.1.1. Surfactant Templates

Template-directed synthesis is currently the most widely used method to fabricate mesoporous materials because of its versatility. Numerous surfactant templates have been used to fabricate mesoporous structures, including cationic surfactant, anionic surfactant, non-ionic surfactant and polymeric surfactants. All of these surfactants are bifunctional molecules that contain a lyophilic head group and a lyophobic tail [14]. Such amphiphilic nature is the main reason that surfactants can associate into supramolecular arrays.

The extent of micellization, the shape of the micelles, and the aggregation of micelles into liquid crystals depends on the surfactant concentration. For example, cetyltrimethylammonium bromide ($CH_3(CH_2)_{15}N(CH_3)^{3+}Br^-$ or $C_{16}TMABr$) in water will form spherical micelles that contain *c.a.* 90 molecules [14]. In the micelle, the hydrophilic head groups form the outer surface and the hydrophobic tails point toward the center. This arrangement minimizes the unfavorable interaction of the tails with water but introduces a competing unfavorable interaction, the repulsion of the charged head groups. The balance between these competing factors determines the relative stability of the micelles.

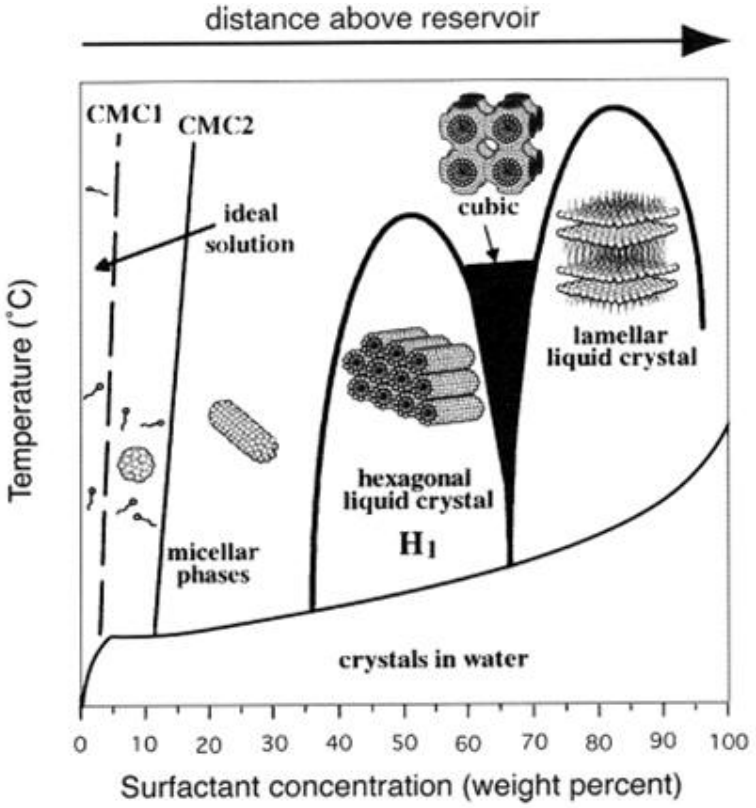

Figure 1.1 The phase diagram of cationic surfactant CTAB in aqueous solution [14].

In a simple surfactant-water system, the relationship between the activity of surfactant and its concentration is schematically shown in Figure 1.1 [14]. At low concentrations, they energetically exist as monomolecules. When increasing concentration, surfactant molecules aggregate together to form micelles in order to decrease the system entropy. The initial concentration threshold at which monatomic molecules aggregate to form isotropic micelles is called CMC (critical micellization concentration). When the concentration keeps increasing, hexagonal close packed arrays appear, producing the hexagonal phases. The next step after that is the coalescence of the adjacent, mutually parallel cylinders to produce the lamellar phase or cubic phase.

1.1.2. Formation Mechanism

Liquid crystal templating (LCT) mechanism MCM-41 possesses a regular hexagonal array of uniform pore sizes with a broad spectrum of pore diameters between 150 and 1000nm [7]. The mesoporous structure can be controlled by a sophisticated choice of surfactants, adding auxiliary organic chemicals and changing reaction parameters. And since the surfactant templating is different with the traditional single organic molecule or metal ion templating, the mechanisms of the formation of MCM-41 have attracted much attention.

Beck et al. originally proposed the liquid crystal templating mechanism (LCT) [7, 15, 16], based on the similar microscopy and X-ray diffraction results of MCM-41 and the liquid crystal formed by isolated surfactant. They consider the liquid crystal as the template to form mesoporous MCM-41. In this mechanism, there are two possible pathways as schematically show in Figure 1.2: (1) the liquid crystal mesophases may form prior to the addition of silicate species; (2) the silicate species added to the reaction mixture may influence the ordering of the isotropic rod-like micelles to the desired liquid crystal phase, i.e., hexagonal mesophase.

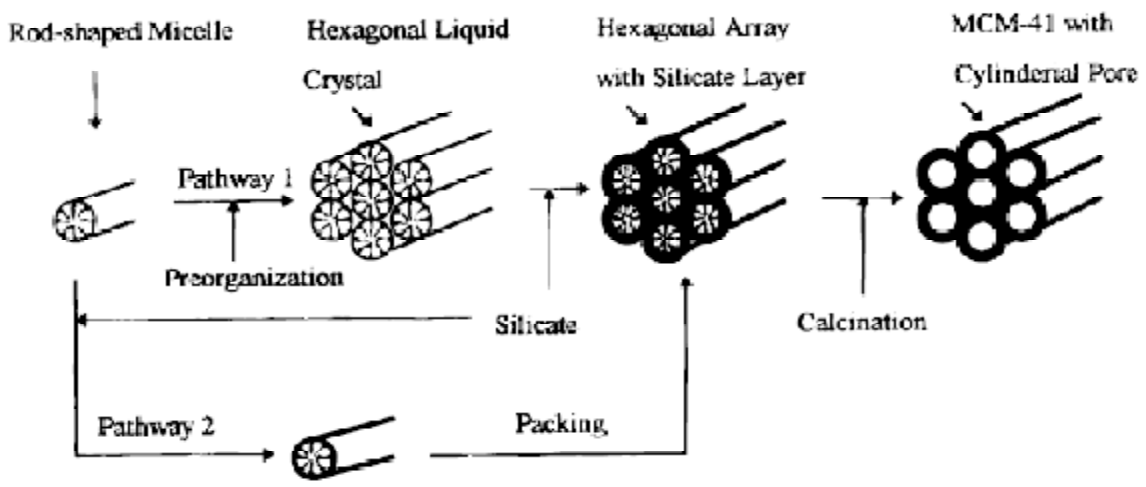

Figure 1.2 Schematic model of liquid crystal templating mechanism via two possible pathways [7].

However, more detailed analysis using XRD, ^{29}Si NMR, *in situ* ^{14}N NMR and thermogravimetric analysis (TGA) has proved that no hexagonal liquid crystalline mesophases exist either in the synthesis gel or in the surfactant solution [17]. It was, therefore, concluded that formation of MCM-41 hexagonal phase is possibly *via* pathway 2, i.e. the addition of the silicates results in the ordering of the subsequent silicate-encaged surfactant micelles. Nevertheless, the concentration of surfactant used in practical synthesis is far lower than the required concentration to form liquid crystal phase. For example, in the synthesis of MCM-41, the concentration of the surfactant CTAB is only 2%. The concentration required to form hexagonal phase is 28% and cubic phase is 80%. The LCT mechanism seems to be plausible. However, the LCT mechanism is still a powerful theory which can provide guidance in practical work.

Cooperative formation mechanism In many cases a "cooperative self-assembly" can take place in situ between the templates and the mineral network precursors yielding the organized architectures (Figure 1.3) [18]. Different with the LCT mechanism that supports the existence of liquid crystal phase of surfactant, this strategy is based on synergic assembly, which is governed by charge density, coordination state and steric chemistry.

Due to the electrostatic interaction between the highly charged anionic silicate species and the positively charged surfactant hydrophilic groups, a lamellar phase would form initially in

the synthesis system [18, 19]. Then the initiation of the silica condensation process reduces the negative charge density of the anionic silicate oligomers. In order to keep the electroneutrality, the hybrid inorganic-surfactant interface begins to develop a more marked curvature, causing the transformation from lamellar to hexagonal phase.

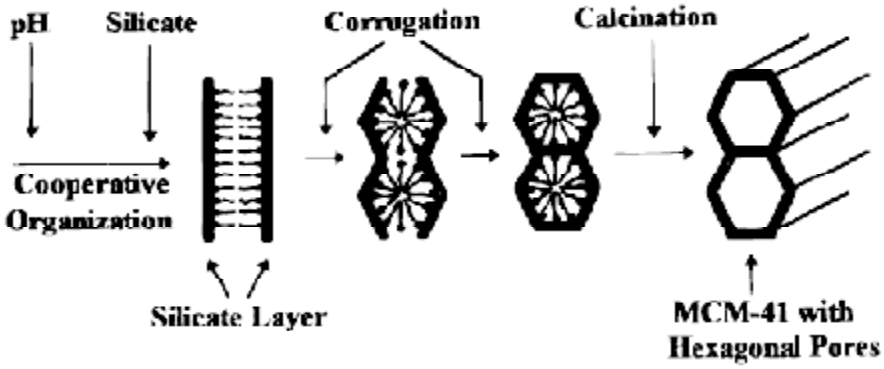

Figure 1.3 Schematic model for transformation mechanism from lamellar to hexagonal phase [18].

The cooperative formation mechanism is a generally accepted theory which can also provide guidance to practical work. It has been continuously supplemented and consummated by following researchers. Stucky et al. studied different inorganic-organic systems and proposed four synthesis routes, viz. S^+I^+, S^-I^+, $S^+X^-I^+$ and $S^-X^+I^-$. Later on, two other synthesis route S^0I^0 and $S^0(IX)^0$ were proposed (Figure 1.4) [2]. Based on the transformation theory, many mesostructured materials with a variety of composition and pore structures were fabricated. The cooperative formation mechanism also shows the importance of properly choosing surfactant to adapt the interaction with inorganic species.

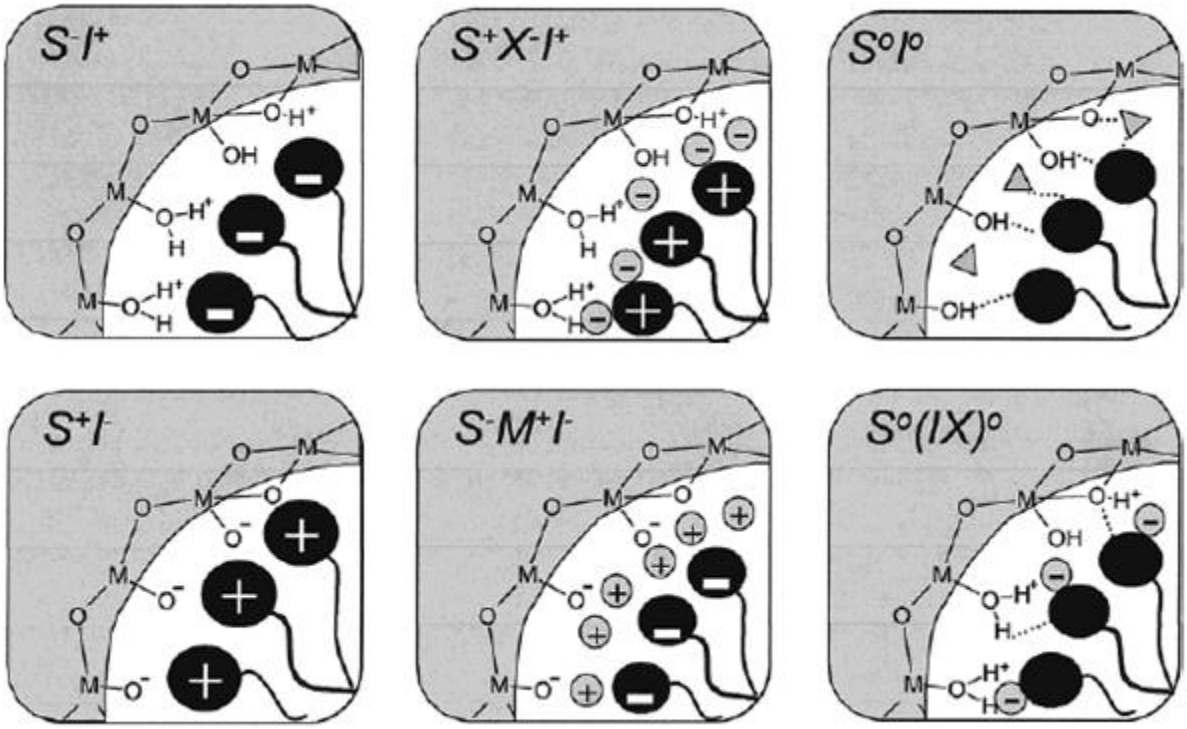

Figure 1.4 Schematic representation of the different types of silica-surfactant interfaces [2].

1.1.3. Thermodynamics

The tenet of the synthesis of MCM-41 silica, either through LCT mechanism or cooperative formation mechanism, is to achieve a well-defined segregation of hydrophobic (organic) and hydrophilic (inorganic) domains at the nanometric scale. From a thermodynamic point view, the hybrid interface plays an important role in the synthesis. The free energy of mesostructure formation (ΔG_{ms}) is composed of four main terms [19], which represent, respectively, the contributions of the inorganic-organic interface (ΔG_{inter}), the inorganic framework (ΔG_{inorg}), the self-assembly of the organic molecules (ΔG_{org}), and the contribution of the solution (ΔG_{sol}).

$$\Delta G_{ms} = \Delta G_{inter} + \Delta G_{inorg} + \Delta G_{org} + \Delta G_{sol} \quad (1.1)$$

The liquid crystal mechanism supports the existence of liquid crystal of organic surfactant, so the contribution due to the self-assembly of the organic molecules prevails over the other factors; while the cooperative formation mechanism proposes the cooperative self-

assembly of hybrid inorganic-organic interface, so the contribution due to that is dominating. In principle, ΔG_{inorg} should be less than ΔG_{inter} or ΔG_{org} in order to make sure the formation of ordered aggregates.

In addition, the formation of mesostructures is controlled by the balance between multiple thermodynamic and dynamic processes [20]. Figure 1.5 shows the interrelationship between the three main components in the mesostructural formation process (template, inorganic species and solvent). It can be seen that there are three steps during the formation process: sol-gel process between inorganic species and solvent, self-assembly process between template and solvent and the formation process of hybrid interface between inorganic species and template.

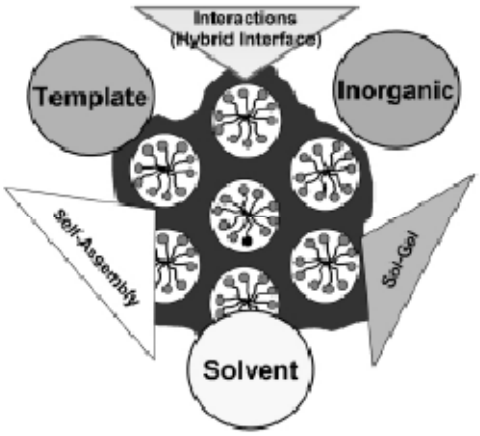

Figure 1.5 The interrelationship between solvent, template and inorganic species [20].

The thermodynamic analysis can help explain the interaction between solvent and template, and even between inorganic species and template [21, 22]. However, because of the complicated compositions of inorganic groups, their properties are determined by dynamics too, usually by the inorganic condensation process, which is directly related to the parameters of solvent such as PH, concentration and catalyst, etc [23].

1.2. Sol-gel synthesis of ordered mesoporous oxides

Currently, the synthesis methods of mesoporous materials are focused on sol-gel method, gas phase method and hydrothermal synthesis method, etc. Sol-Gel process is a method to form glass material through inorganic precursor condensation [23, 24]. The fundamental property of the sol-gel process is that it is possible to generate ceramic material at a temperature close to room temperature. Therefore such a procedure opened the possibility of incorporating in these glasses soft dopants, such as fluorescent dye molecules and organic chromophores [25, 26]. The sol-gel process also provides new approaches and a better control at molecular level [27].

The starting materials used in the preparation of the "sol" are usually inorganic metal salts or metal organic compounds such as metal alkoxides, which have organic ligands attached to the center metal atom. In a typical sol-gel process, reactive metal alkoxides are initially hydrolyzed, followed by condensation and polymerization reactions to form a colloidal suspension, or a "sol". Further processing of the "sol" enables one to make ceramic materials in different forms, such as thin films, wet gel and aerogel, etc [27]. The hydrolysis and condensation processes are as below:

$$\sim MOR + H_2O \rightarrow \sim MOH + ROH \quad (1.2)$$

$$\sim MOH + \sim MOR \rightarrow \sim M - O - M\sim + ROH \quad (1.3)$$

$$\sim MOH + \sim MOH \rightarrow \sim M - O - M\sim + H_2O \quad (1.4)$$

Also, it is possible to have coordination reaction:

$$\sim MOR + R'OH \rightarrow \sim M - OR' + ROH \quad (1.5)$$

There are many factors (e.g. precursor, solvent, catalyst, PH, reaction temperature and hydrolysis rate, etc.), which can affect the hydrolysis rate and condensation rate, and consequently affect the microstructure of the gel network. For instance, the hydrolysis rate increases with the increase of the size of the precursor group [28, 29]. In the silica system, low PH favors the formation of linear oligomers, while under alkaline condition high degree polymers tends to form [30].

The sol–gel processing method has been used for producing metal oxide and ceramic powders with high purity and high homogeneity for many years. The sol–gel route offers a degree of control of composition and structure at the molecular level.

1.3. Encapsulation of Germanium semiconductor clusters

The development of mesoporous materials has provided new pathways for the formation of nanostructured host/guest compounds. The interesting points are the effects of constrained matrices on the activity of incorporated semiconductors. Due to their high surface areas, uniform pore sizes and highly ordered pore structures, MCM-41 silicas are ideally suited for loading semiconductor nanoparticles [31-35] which have potential optoelectrical applications [36, 37]. The optoelectronic properties of semiconductor quantum dots (QDs) depend on their particle size due to quantum confinement effect and interfacial dielectric confinement.

There are many strategies for incorporation of semiconductors into ordered porous silica matrices, such as simple physisorption [38], electrostatic interaction [39] and covalent attachment of organic ligands to the mesoporous matrices [40]. Fabrication techniques by ion exchange, molecular diffusion and solution reaction inside the pores are usually called “ship in the bottle” [41]. This method is simple and convenient but removing the solvent molecules from the host pores is difficult. Methods involving gaseous precursors [42-44] usually rely on expensive precursors and complicated equipment. And the loading efficiency still needs to be improved. So it is important to develop new fabrication techniques for loading semiconductor nanoparticles.

1.4. Scope and Objectives

The ordered pore systems of MCM-41 silica can serve as size limiting and stabilizing matrices for the formation of semiconductors. The silica-wall structure of the host MCM-41 silica with large band gap can serve as a barrier between the nanostructures. Besides, the synthesis of nanoparticles in the mesopores of MCM-41 silica provides a very effective way to obtain monodisperse products.

The first objective of this study is to synthesize suitable host MCM-41 silica through an extremely low concentration route and to investigate the experimental parameters for morphology control. The synthesis system is relatively simple and we focus on the morphology control of the as-synthesized MCM-41 particles by varying the experimental conditions. The goal is to find a suitable MCM-41 host with highly ordered pores system, uniform pore size and large particle size for the encapsulation of semiconductor nanoparticles. Then the following work will focus on the incorporating Ge semiconductor nanoparticles into the host networks. The evaluation of loading efficiency will also be conducted through different characterization methods.

CHAPTER 2 EXPERIMENTAL

2.1. Chemical Reagents

Generally, the mixture of surfactant and silica source is present in the alkaline synthesis media initially. In this study, Hexadecyltrimethylammonium (CTAB) was used as the cationic surfactant, while tetraethyl orthosilicate (TEOS) served as the silica source. Aqueous sodium hydroxide or ammonia was used as the catalyst. The chemicals used in this study are listed in table 2.1.

Table 2.1 Chemical reagents used in this study

Reagent	Molecular formula	Purity	Manufacture
Hexadecyltrimethylammonium bromide	$C_{16}H_{33}(CH_3)_3N^+Br^-$	A.R.	Aldrich
Tetraethyl orthosilicate	$Si(OC_2H_5)_4$	A.R.	Aldrich
Sodium hydroxide	NaOH	A.R.	Aldrich
Ammonia	$NH_3 \cdot H_2O$	A.R.	Aldrich
Germanium tetrahydride	GeH_4	A.R.	Aldrich
Ethanol	CH_3CH_2OH	A.R.	Aldrich

2.2. Synthesis Techniques

2.2.1. General Techniques to synthesis MCM-41

Typically, the silica source (e.g., tetraethylorthosilicate) is added to a clear alkaline aqueous solution containing micelle-forming surfactant and PH adjustment catalyst (e.g., Sodium hydroxide or ammonium hydroxide) under constant stirring. In this study, CTAB, which have a hydrophilic headgroup and a hydrophobic tail group, were used as the mesostructure directing agents. When the hydrolysis process is triggered, the silica source starts to form multidentate, multicharged anions, which can cooperatively interact with the surfactants to assemble into a silica-surfactant phase and further form crystalline solid. The typical procedures are listed below:

1) At room temperature, 4 g of hexadecyltrimethylammonium bromide (CTAB) was dissolved in 540 ml of distilled water under vigorous stirring

2) 410 ml of aqueous ammonium (25%) was added to the solution and the temperature was raised to 341 K

3) 20 ml of TEOS was added dropwisely to the solution, forming white precipitates

4) The reaction was performed at 341 K under strong stirring for 2h

5) The white products were filtered, washed with distilled water and dried in an air oven at 314 K for future use.

2.2.2. Encapsulation of Ge nanoparticles into MCM-41

Three different methods for incorporating Ge semiconductor nanoparticles into MCM-41 networks have been investigated. The detailed synthesis procedures are listed as below:

Method 1: H_2 reduction

1) The host mesoporous silicate were calcined at 823 K for 4 h to remove the surfactant molecules and other organic species in the channels of MCM-41

2) 2 ml of $GeBr_4$ was added in 5 ml of THF solution under strong stirring

3) MCM-41 powders were placed in a three-neck flask and vacuum dried for 15 min

4) At room temperature, the $GeBr_4$ solution was impregnated into to flask very quickly until the powders were completely immersed in the solution, and then argon flow was introduced into the system

5) Repeat the vacuum drying and impregnation step 2-3 times until the color of MCM-41 powders turned from white to red-orange

6) The powders were placed in a quartz container and transferred to a tube furnace. Under constant hydrogen flow, the furnace was heated up to 823 K for 10 h, and then 873 k for 30 min

7) After the sample was cooled down to room temperature, its color turned to black-gray and can be used for future characterization.

Method 2: Chemical vapor infiltration and pyrolysis

1) The host mesoporous silicate were calcined at 823 K to remove the surfactant molecules and other organic species in the mesopores channels

2) As-prepared MCM-41 hosts were placed in a quartz container in a tube furnace

3) The samples were thermally dehydrated under vacuum at 423 K for 4 h

4) Germaniumtetrahydrid gas was constantly introduced through the chamber at room temperature for 1 h

5) The reaction chamber was heated up to 823 K leading to pyrolysis of the GeH_4 to form Ge nanoparticles

6) The sample was vacuum dried at room temperature to remove residual GeH_4 and H_2 gases

7) The sample was washed by deionized water and ethanol, followed by annealing in static vacuum at 973 K for 1-2h.

Method 3: Na-Naphthalene reduction

1) The host mesoporous silicate were calcined at 823 K to remove the surfactant molecules and other organic species in the mesopores channels

2) MCM-41 powders were transferred to a three-neck flask and vacuumed for 15 min to remove the air inside the pore system

3) 1 ml of the precursor $GeBr_4$ were dissolved in THF, and then impregnated into the flask under vacuum

4) To initiate the growth of Ge nanoparticles, 2 ml of 1 M solution of Sodium-Naphthalene in tetrahydrofuran was injected into the flask. The reaction was remained at room temperature for 1 h. In the course of the reduction the color of the solid changed from white to yellow-orange

5) Ge-filled MCM-41 composite was collected as a powder by filtering it from the reaction mixture

6) The sample has a grey color and was wash with dry tetrahydrofuran and deionized water to remove the Ge at the outer surface of MCM-41

7) The washed MCM-41 loaded with Ge nanoparticles was vacuum dried and characterized by various analytical techniques.

2.3. Analysis and Characterization

2.3.1. X-ray Powder diffraction (XRD)

X-ray powder can be used to investigate the structure and crystallinity of the MCM-41 particles. The XRD patterns of all samples were measured with a Phillips-X'PERT X-ray powder diffraction system (Cu, K_α= 1.5406 Å). The data collection and analysis were carried out using the software supplied with the diffractometer. The size of the particles can be estimated by the Scherrer equation: $D_c=K\lambda/\beta cos\theta$.

2.3.2. Transmission Electron Microscopy (TEM)

All transmission electron microscopy was performed using a JEOL 2010 electron microscope operated at 200 kV. Samples for the TEM measurement were suspended in ethanol and one drop of the dispersion was placed on a graphite foil on a copper grid and allowed to dry, leaving the crystallites in random orientation on the foil.

2.3.3. Energy Dispersive Spectroscopy (EDS)

Elemental analysis was carried out using an EDAX attachment on a JEOL 2010 TEM with the electron beam focused to two nanometers. EDS is a technique used to identify the elemental composition of a sample or small area of interest on the sample. During the examination process, a solid-state detector is used to collect the characteristic X-rays emitted from a sample. By analyzing the emitted X-rays, the elemental composition of the sample can be determined. A collection of X-ray energies from 0 to 40 KeV can be collected and displayed on a computer screen. Peaks will show up on the spectrum, corresponding to energies of elements

present in the sample. The area included within a peak is roughly proportional to the amount of the corresponding element in the sample, although the detector efficiency decreases with increasing energy. The EDS system can be used for quantitative analysis by counting the X-rays received in the channels that correspond with a peak of interest. EDS is a powerful tool for microanalysis of elemental constituents.

2.3.4. Scanning Electron Microscope (SEM)

SEM was used to characterize the structures and morphologies of the processed particles. SEM experiments were performed on dry powders with a LEO 1530 SEM with a field emission gun without sample sputtering.

2.3.5. N_2 absorption and desorption

Adsorption and desorption isotherms for nitrogen were obtained at 77K using a Micromeritics ASAP-2010. The samples were outgassed at 573K for 12h before measurements were performed. Specific surface area values were obtained using the BET (Brunauer-Emmett-Teller) equation. The pore size distribution data was obtained using the BJH (Barrett-Joyner-Halenda) method.

CHAPTER 3 PREPARATION OF THE MESOPOROUS SILICA WITH VARIOUS MORPHOLOGIES

In the past decade, a great amount of work has been dedicated to the synthesis of mesoporous silica material. Different mesostructures have been synthesized through many different strategies, such as MCM-41 [7], SBA-15 [10], MSU-1 [11] and etc. The synthesis process has been well developed as well as the mechanism explanation, which can provide fundamental guidance to the fabrication work. Some important discoveries with respect to the morphology control of MCM-41 are listed below:

(1) Ozin and co-workers [45] first demonstrated the co-presence of various morphologies of mesoporous silicates particles under acidic conditions. The materials were synthesized in an extremely dilute solution of TEOS and surfactant with very low pH conditions.

(2) Huo et al. [46] demonstrated that mesoporous silica could be produced in the form of marblelike spheres of about 1 mm in diameter. The size of the spheres was reported to be controlled by the stirring speed.

(3) Grün et al. [47] reported the synthesis of spherical silica particles featuring the MCM-41 structure, whose size ranged from 400 to 1100 nm. Their synthesis procedure was a modification to Stöber's synthesis [48] of monodisperse silica spheres by adding cationic surfactant to the reaction mixture during the formation of MCM-41.

(4) Büchel et al. [49] reported a novel method for the synthesis of submicrometer-sized (~ 700 nm) solid core/mesoporous shell silica spheres. Their method was based on a combination of the Stöber approach [48], the Unger growth process [50], and the Kaiser approach [51].

(5) Various morphologies of mesoporous silica were reported such as Teraski et al. [52] reported the method for the synthesis of single crystal SBA-16; Cai Q. et al. [53] reported the fabrication of single crystal MCM-41; Lin. H. P. [54] reported the synthesis of thin-film silica.

Although various morphologies have been previously achieved, little is known about the formation of helical, slice and rice-like morphologies of mesoporous silica. Here in, we report the control of morphologies of silica particles, where MCM-41 silica monolith, mesoporous silica slice, rice-like mesoporous silica and helical mesoporous silica are produced through pathways of extremely low surfactant concentrations with a basic medium. The corresponding formation mechanisms were proposed to interpret the morphogenetic control on the basis of deposition of self-assembled silicate rod-like micelles.

3.1 Synthesis of micrometer-sized MCM-41 particles

3.1.1. Synthesis conditions

Typical synthesis of ordered MCM-41 silica particles using surfactant templating were studied here according to the procedure reported in the literature [53]. The ratio of the starting materials is 4 g (CTAB): 540 ml (H_2O): 410 ml ($NH_3 \cdot H_2O$): 20 ml (TEOS). Aqueous ammonia was used as the catalyst and CTAB was used as templating surfactant. Five routes (Table 3.1.) were opted to synthesize the mesoporous MCM-41 with different particle sizes or morphologies.

Table 3.1 Synthesis conditions of MCM-41.

No.	Stirring speed	Reaction Temp. (K)	Time	Seed Crystal	Product
1	Strong	313	2h	None	Sphere
2	Strong	341	4h	Powder	Rod
3	Static	R.T.	3 ~ 4d	Powder	Film
4	Strong	304	12h	Solution	Rice-like
5	Strong	341	2h	EtOH	Helical

3.1.2. Results and discussions

MCM-41 powders synthesized through route 1 were filtered and washed with distilled water, then followed by calcinations in air at 873 K for 4 h. To investigate the morphology of the sample, scanning electron microscopy (SEM) and transmission electron microscopy (TEM) studies were performed on the samples. From the SEM images (Figure 3.1A and B), we observed monodisperse spherical MCM-41 particles with diameters ranging from 0.3 ~ 1 μm and with a hexagonal shape. The SEM images clearly show that the nanoparticles stack compactly and the

average distance of the particle interstices is *c.a.* 100 nm. Figure 3.1B shows that a single crystal of MCM-41 in the shape of hexagon can grow to be as large as $2\times2\ \mu m$ and these hexagonal MCM-41 particles are highly regular in shape.

The microstructures of the as-synthesized MCM-41 are clearly revealed by TEM and HRTEM. Figure 3.2A shows the typical TEM images of the spherical MCM-41 samples, which exhibit a hexagonal external surface morphology. The size of the particles ranges from 400 to 1000 nm, which is close to that obtained from SEM results. TEM images (Figure 3.2B, C, D) of the samples show the existence of highly ordered hexagonal array and streak structural features. The streak is the view of the crystals whose c axis is perpendicular to the line of vision (Figure 3.2B). Figure 3.2C shows the image of a perfect hexagonal single crystal of MCM-41 without intergrowth and twinned aggregation. Enlargement of the crystals (Figure 3.2D) is the view of the crystals whose c axis parallels the line of vision, which clearly reveal the long-range highly ordered mesoporous structures of MCM-41.

We suggest that the formation of the MCM-41 spheres is through the pathway 2 of Liquid Crystal Templating mechanism [7], *i.e.* the nucleation involving silica-surfactant interactions facilitate the assembly of inorganic-organic micelles. During the reaction, we observed that the clear solution turned cloudy immediately after the mixing of surfactant and inorganic solution containing silica precursors. This indicates the formation of inorganic-organic self-assembled silicate micelles (SSMs) through ion exchange of silicate oligomers with Br^- and OH^- anions. Without the presence of silicate oligomer, SSM might not form under the diluting condition [55]. Then during the condensation of the silicate groups on the SSMs, the arrangement and deposition of the micelles are governed by the inside electrostatic interactions and outside experimental conditions such as pH, solvent and stirring speed.

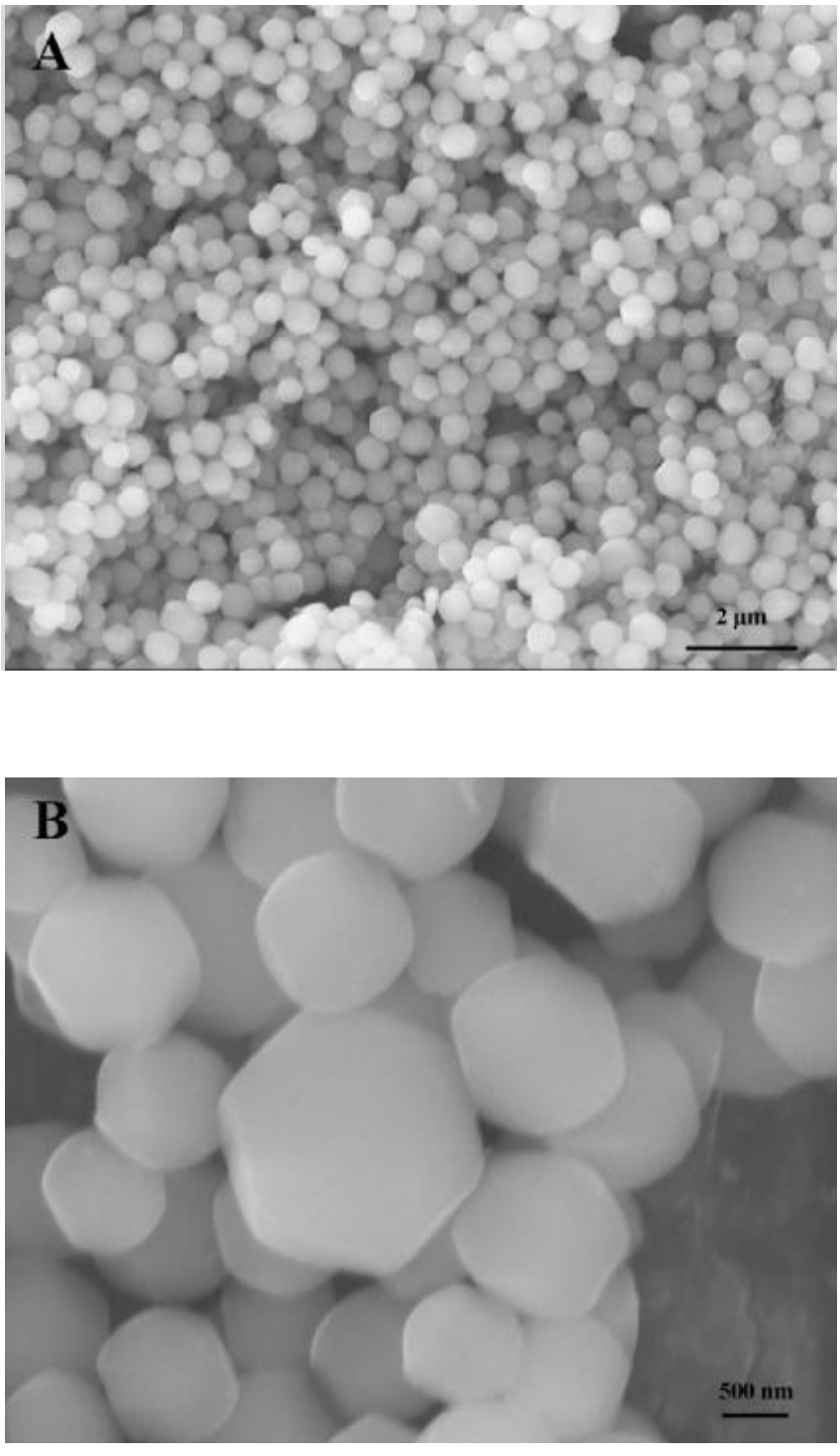

Figure 3.1 SEM images of ordered MCM-41 particles: A) Scale bar, 2 µm. B) Scale bar, 500 nm.

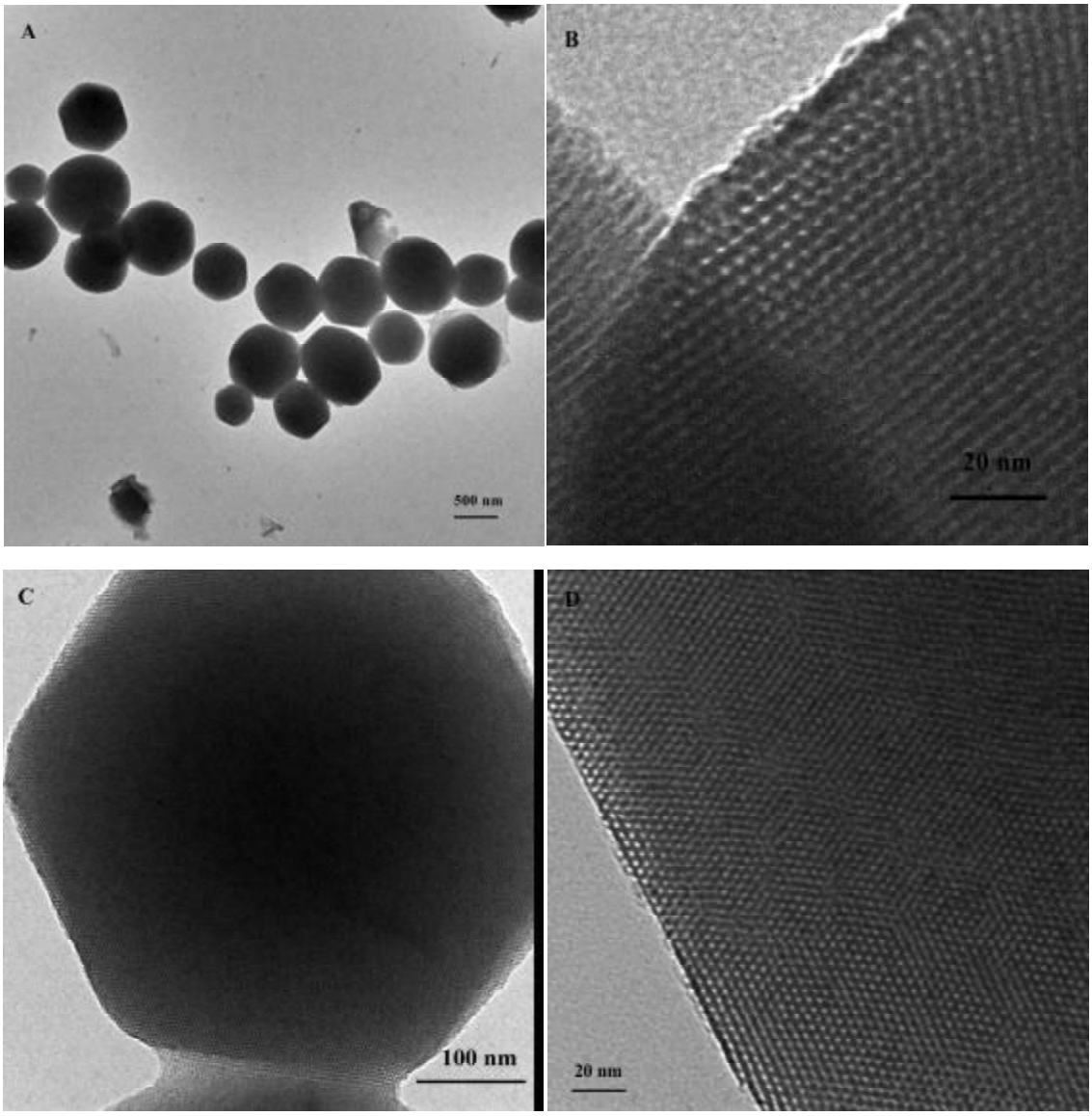

Figure 3.2 TEM images of ordered MCM-41 particles: A) Scale bar, 500 nm. B) Scale bar, 20 nm. C) Scale bar, 100 nm. D) Scale bar, 20 nm).

From the *in situ* particle size development study, it was suggested that monodispersity of the particles is because the particles were generated successively, growing rapidly to the same maximum size one after another under diluting conditions [56]. This is consistent with our synthesis conditions and observed results.

The internal structure of the porous monodisperse silica spheres is dependent on the type of the surfactant. And the length of the surfactant-silicate micelles is determined by the solvent. In this experiment, the solvent containing CTAB and ammonia favors the formation of monodisperse mesoporous silica spheres possessing highly ordered hexagonal regularity. These spherical MCM-41 particles are of great interest for applications in chromatography [57-60] and cosmetics [61].

3.2 Synthesis of large monolith MCM-41 rod

3.2.1. Synthesis conditions

In route 2, we used MCM-41 spherical particles obtained via route 1 as the seed crystal to grow large monolith MCM-41 silica. After the solutions of CTAB and aqueous ammonium were completely mixed under vigorous stirring, the seed crystal was added to the solution. Then the system was heated up to 341 K and the TEOS was added drop by drop. The rest procedures were the same with route 1.

3.2.2. Results and discussions

The seed crystal growth procedures were repeated three times for comparing the effects to particles size and morphology. For the first time of seed crystal growth, we observed that the as-produced particles have a rod shape and the size increases markedly. Figure 3.3 shows the typical SEM images of the monolith MCM-41 rods. It is clearly seen that the length of the rods is *c.a.* 2 μm and the diameter is *c.a.* 1 μm.

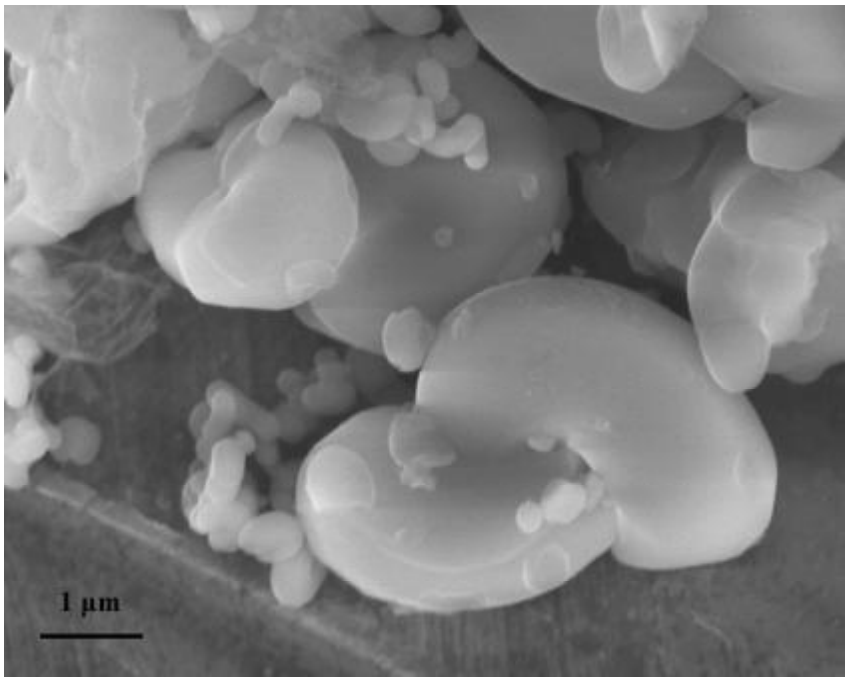

Figure 3.3 SEM images of rod-like MCM-41 from the 1st time of seed crystal growth.

The SEM images of MCM-41 particles from the second time of seed crystal growth are shown in Figure 3.4. The particles obviously increase in size than those obtained from the first time seed crystal growth and the size can be as large as 3×1.5 μm (length$\times$diameter). We also observed that some of the particles from the first time seed crystal growth (Figure 3.3) have a more marked curvature than those showed in Figure 3.4B, which have a perfect rod shape. This may be caused by the charge density change of the anionic silicate oligomers during the condensation process. It is well-known that the ratio of the interaction of the silicate oligomers among the Gouy-Chapman region to that of the hydrocarbon chains resulting from the van der Waals forces is related to the curvature of the formed micelles [62]. The lamellar phase formed initially by highly charged anionic silicate species and the positively charged surfactant hydrophilic groups is electronically neutral. The initiation of the silica condensation process reduces the negative charge density of the silicate oligomers, and then the hybrid inorganic-surfactant interface begins to develop a more marked curvature. This effect can be extended to the macrometric surface of the particles, which have less mechanical strength and thus bend easily. When the particles obtained from the first time seed crystal growth were used as seed again in the second time, the system was maintained at 341 K for 1 h before adding TEOS.

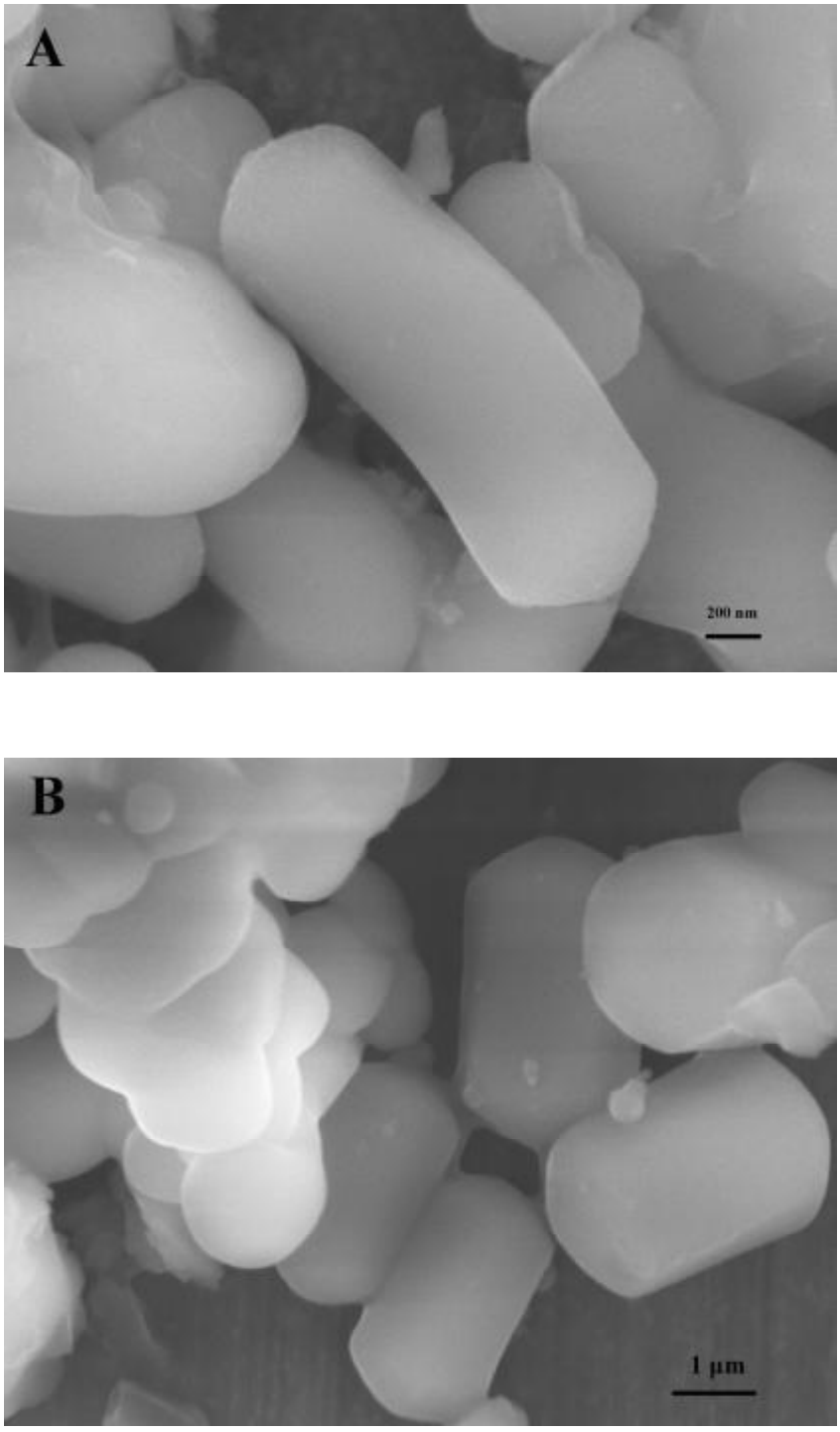

Figure 3.4 SEM images of rod-like MCM-41 from the 2nd time of seed crystal growth.

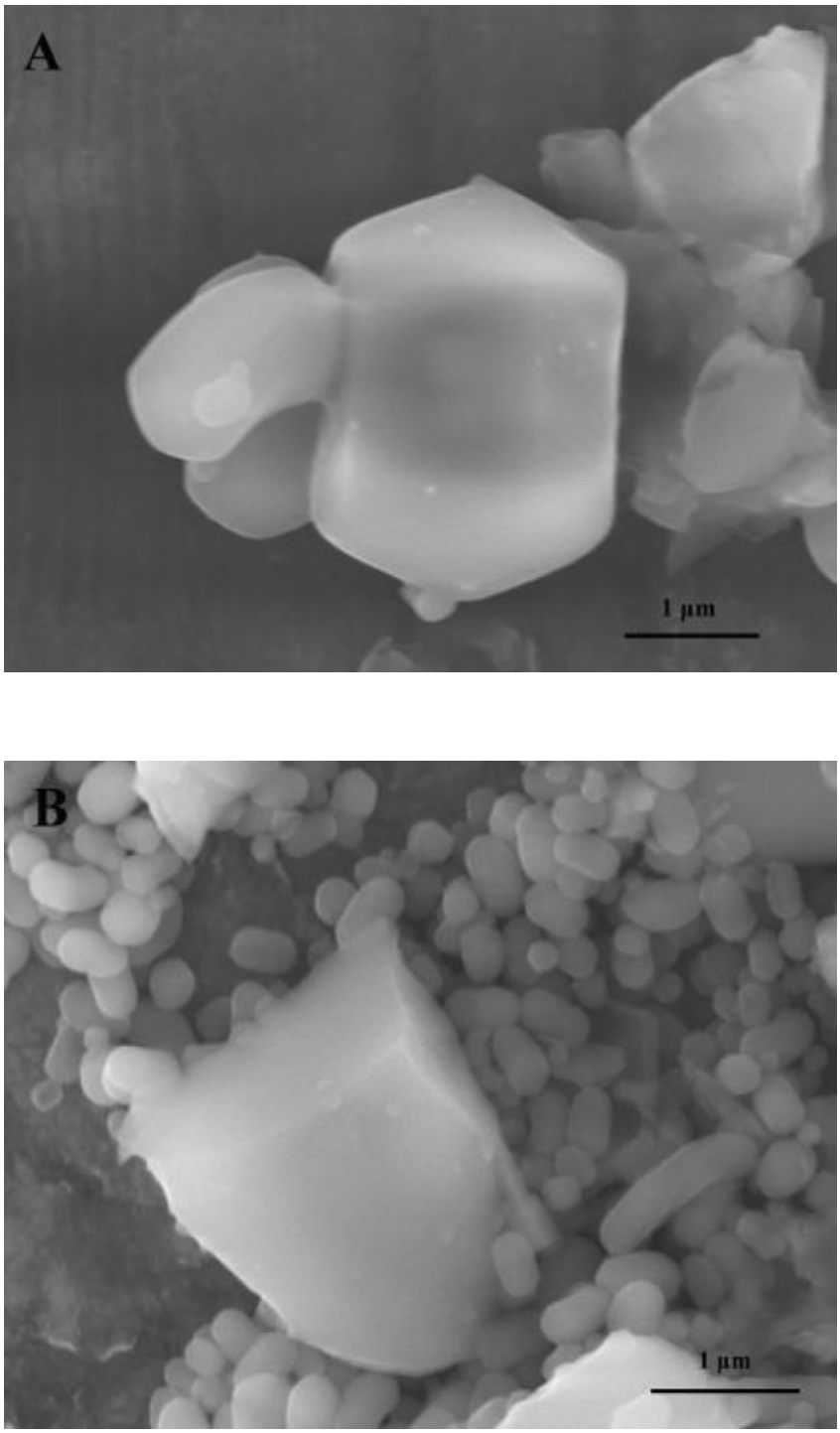

Figure 3.5 SEM images of MCM-41 rod from the 3rd time of seed crystal growth.

Consider the reaction equilibriums in the nucleation process (Equation 3.1, 3.2 and 3.3). In conditions where the concentration is low and the pH is high, the equilibrium may shift backward to dissolve MCM-41 particles. We found that at this temperature, the particles would dissolve in the solution very slowly and remove the irregular array on the surface. This process can polish the surface of the particles, which can be used as seed crystal for the next step of nucleation and growth.

$$\sim SiOR + H_2O \leftrightarrow \sim SiOH + ROH \quad (3.1)$$

$$\sim SiOH + \sim SiOR \leftrightarrow \sim Si - O - Si\sim + ROH \quad (3.2)$$

$$\sim SiOH + \sim SiOH \leftrightarrow \sim Si - O - Si\sim + H_2O \quad (3.3)$$

However we didn't observe obvious change for the third time of seed crystal growth (Figure 3.5). The shape and size of MCM-41 rod are similar with those shown in Figure 3.4. This indicates that there is a size limit for the growth of the crystal. When the limit has been reached, the particles would prefer to form new crystal nucleus instead of growing on the existed particles. This has been proved by the concomitant small particles (Figure 3.4B) with an average size of 500 nm.

3.3 Synthesis of MCM-41 film

3.3.1. Synthesis conditions:

According to synthesis route 3 (Table 3.1), 410 ml of ammonia (25%) solution was mixed with 540 ml of distilled water. Then 4.0 g of surfactant (CTAB) was added to the solution with vigorous stirring. The mixture was heated up to 341 K and 10.0 g of the spherical MCM-41 particles obtained in section 3.1 was added to the solution. The synthesis system was maintained at 341 K until MCM-41 particles were completely dissolved, and then cooled down to room temperature. The system was maintained in static conditions for 3 ~ 4 days. The white precipitates appeared on the surface the solution were filtered, washed with distilled water and dried in air oven for future characterization.

3.3.2. Results and discussions

Through this static growth method, MCM-41 films with thickness from tens of nanometers up to about 300 nm have been synthesized at the air-liquid interface. The sample was collected directly from the synthesis solution and characterized by SEM. Figure 3.6A clearly shows the SEM images of the continuous and transparent MCM-41 films with a thickness of only about 0.1 nm. It has a smooth surface and very strong mechanical strength. The sample was filtered by a Buchner funnel and still remains the integrality of the film morphology (Figure 3.6B).

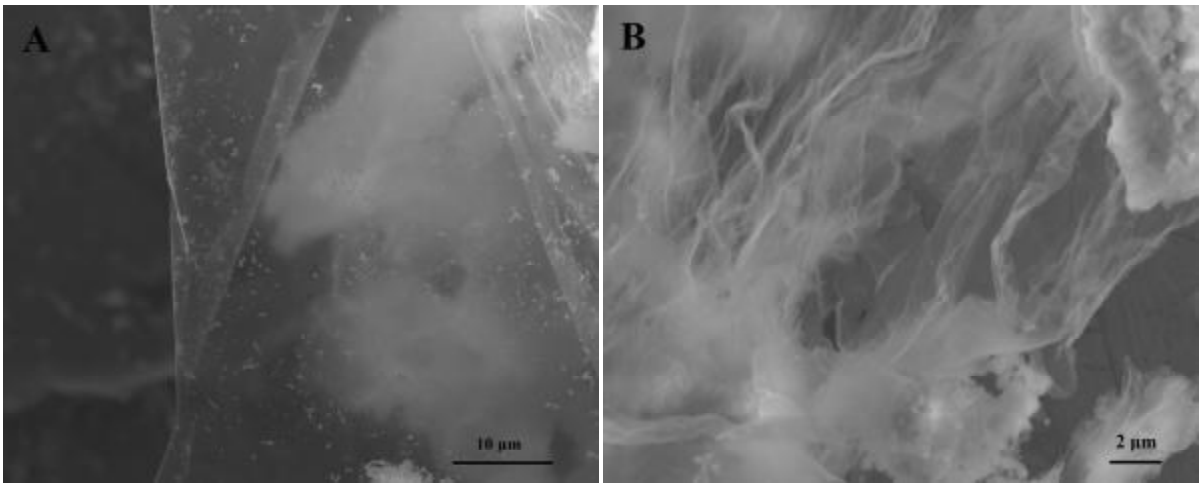

Figure 3.6 SEM images of MCM-41 thin film. A) the sample was collected directly from the synthesis solution. B) the sample was collected after filtration.

Figure 3.7 shows the SEM images of MCM-41 films with thicknesses of about 300 nm. Most of MCM-41 films are stacking together (Figure 3.7A). Figure 3.7B shows that the films have smooth surfaces. The film surface growing into the solution shows roughness on the mesoscopic scale (Figure 3.7C), which might represent a silica replica of the disposition of micellar structures as they are deposited at this lower surface.

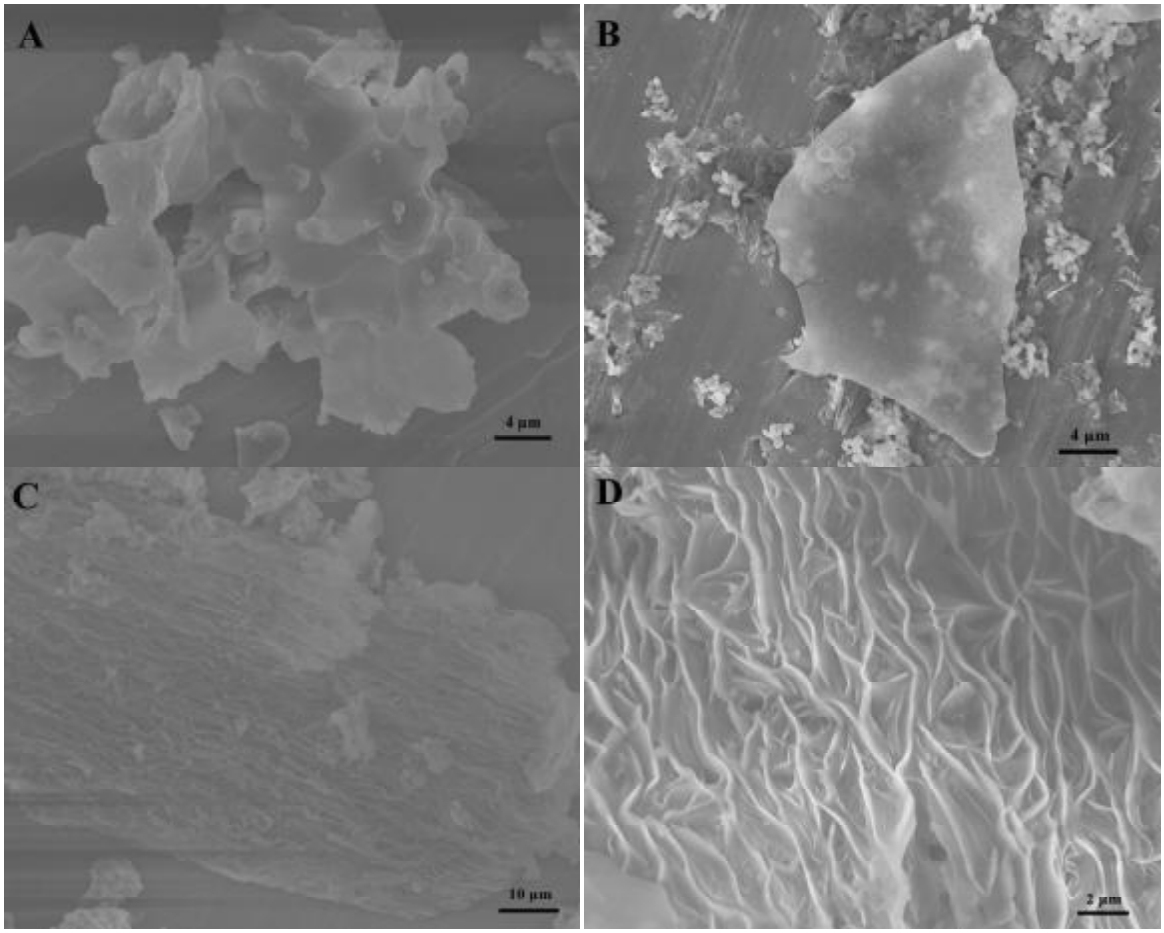

Figure 3.7 SEM images of MCM-41 films with thickness of about 300 nm: A) Scale bar, 4 μm. B) Scale bar, 4 μm. C) Films immersed in the solution. D) Films dispersed in ethanol.

When the sample was dispersed in ethanol, a wrinkle structure can be seen on the surface (Figure 3.7D). This implies that ethanol will destroy the smoothness of the surface of MCM-41 films.

It was proposed that the surfactant was used as template at the interface between air and water for the deposition of silicates to form mesoporous MCM-41 silica [63]. The dissolved MCM-41 particles are in equilibrium with the synthesis solution, which may form surfactant-silicate micellar aggregates in the solution, which may further form MCM-41 mesostructures through condensation and polymerization processes. The surfactant micelles at the interface of the solution and air react differently with those immersed in the solution. With extremely low concentration, the head groups of the surfactant micelles at the air-liquid interface may be in

equilibrium with the synthesis solution, thus the arrangement of the micelles at the air-liquid interface may be in the form that the micelle rods are parallel to the interface.

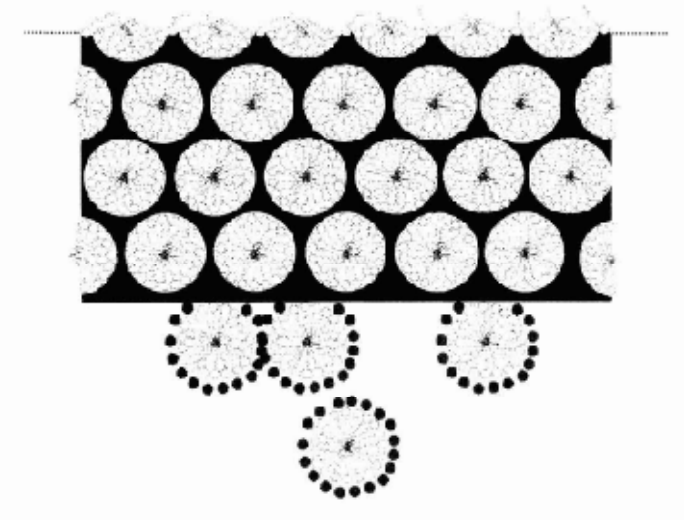

Figure 3.8 Graphical illustration of the proposed mechanism for the formation of mesoporous silica film at the air-water interface [63].

After a long time (3 ~ 4 days) of self-assembly of the surfactant-silicate mecelles under static conditions, the upper surface of the film was dissolved by the synthesis solution and appeared as a smooth surface. By contrast, the surfactant-silicate might randomly deposit on the lower surface of the film and thus showed a rough structure.

3.4 Synthesis of uniform rice-like MCM-41 particles

3.4.1. Synthesis conditions:

After MCM-41 particles synthesized in section 3.1 were filtered, the rest synthesis solution was also collected as the reaction solution here. 410 ml of ammonia (25%) solution, 4.0 g of surfactant (CTAB) and 540 ml of collected solution were mixed under vigorous stirring at 341 K. The system was cooled down to 308 K. 10 ml of TEOS solution was added to the system very slowly by a syringe pump (12 h). The temperature was 300 K after the reaction was completed and the products were filtered, washed by distilled water and dried in an air oven.

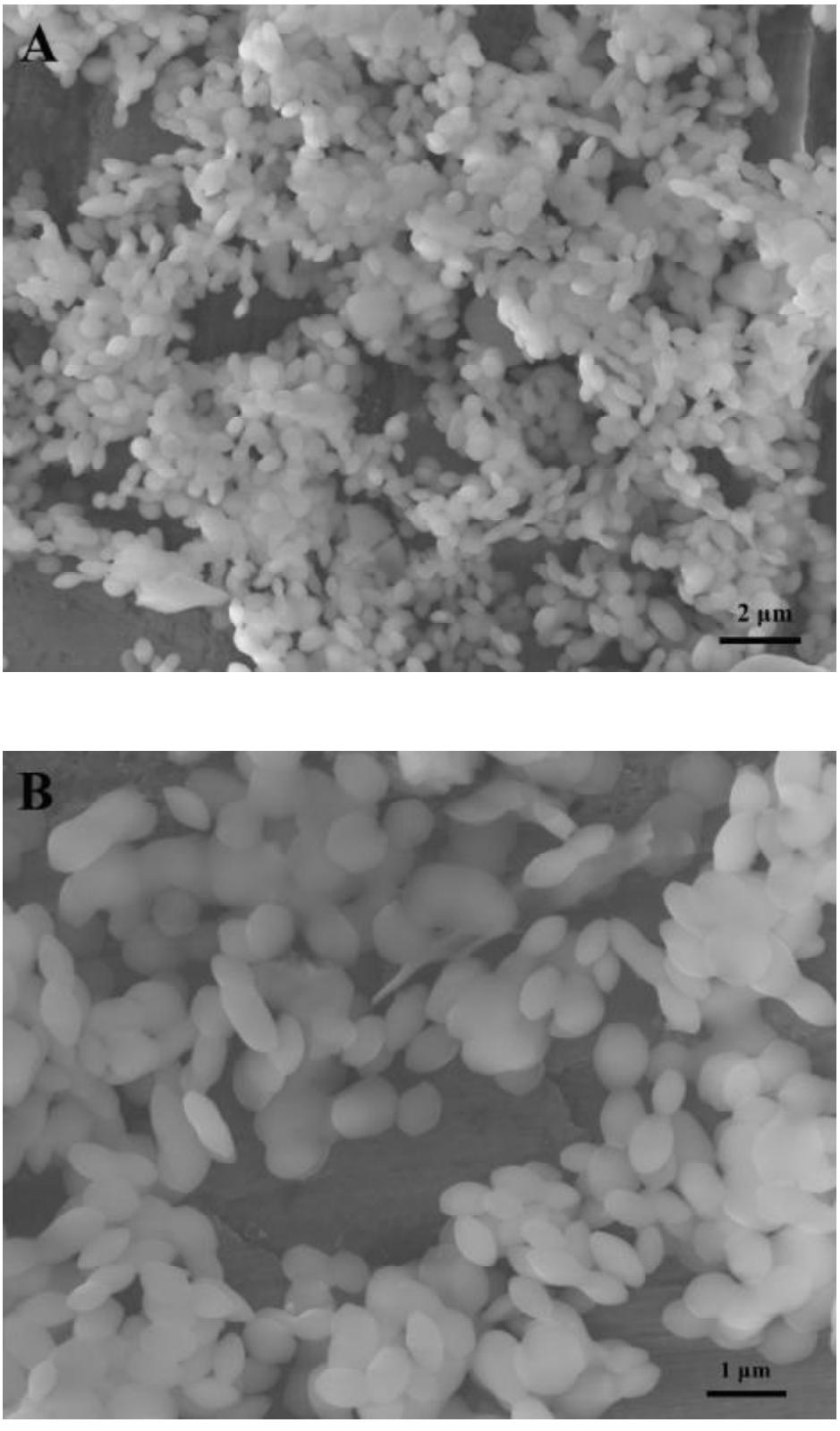

Figure 3.9 SEM images of rice-like MCM-41 particles.

3.4.2. Results and discussions

The SEM images of as-synthesized MCM-41 particles are show in Figure 3.9. The length of the rice-like particles ranges from 300 ~ 600 nm and the average diameter is about 300 nm. We suggest that the suspended silicate species in the reaction solution provide nucleation sites for the formation of new MCM-41 crystal. After the silica precursor was introduced into the solution, the crystallization process happened very quickly due to the existence of many nucleation sites. Because the nucleation sites are homogeneously distributed in the solution, the interaction between the surfactant micelles and the silicate species completed in a very short time in this supersaturated solution, which prefers the formation of many small sized rice-like MCM-41 particles.

3.5 Synthesis of helical MCM-41 silica

3.5.1. Synthesis conditions:

In this synthesis route, before adding the TEOS solution, 10 ml of EtOH solution was added to the synthesis system. The reaction was performed at 341 K under strong stirring for 2 h. The products were collected after filtration.

3.5.2. Results and discussions

Many helical MCM-41 silicas were observed by SEM (Figure 3.10). A possible explanation for the formation of helical MCM-41 can rely on the slow gelation process. The existence of the EtOH solution slows down the hydrolysis and condensation processes of silicate, causing the co-existence of liquid sol phases and solid gel phases. During the filtration process, the interaction between the sol and gel caused by the filtration pressure helps to form the helical MCM-41.

3.6 Summary

The key point in the sol-gel synthesis of mesostructured silica is to thoroughly adjust the chemical, spatial and structural properties of the templating surfactant. Prior to obtain well-defined textured mesostructures, sufficient tailoring to the inorganic-organic interface is required.

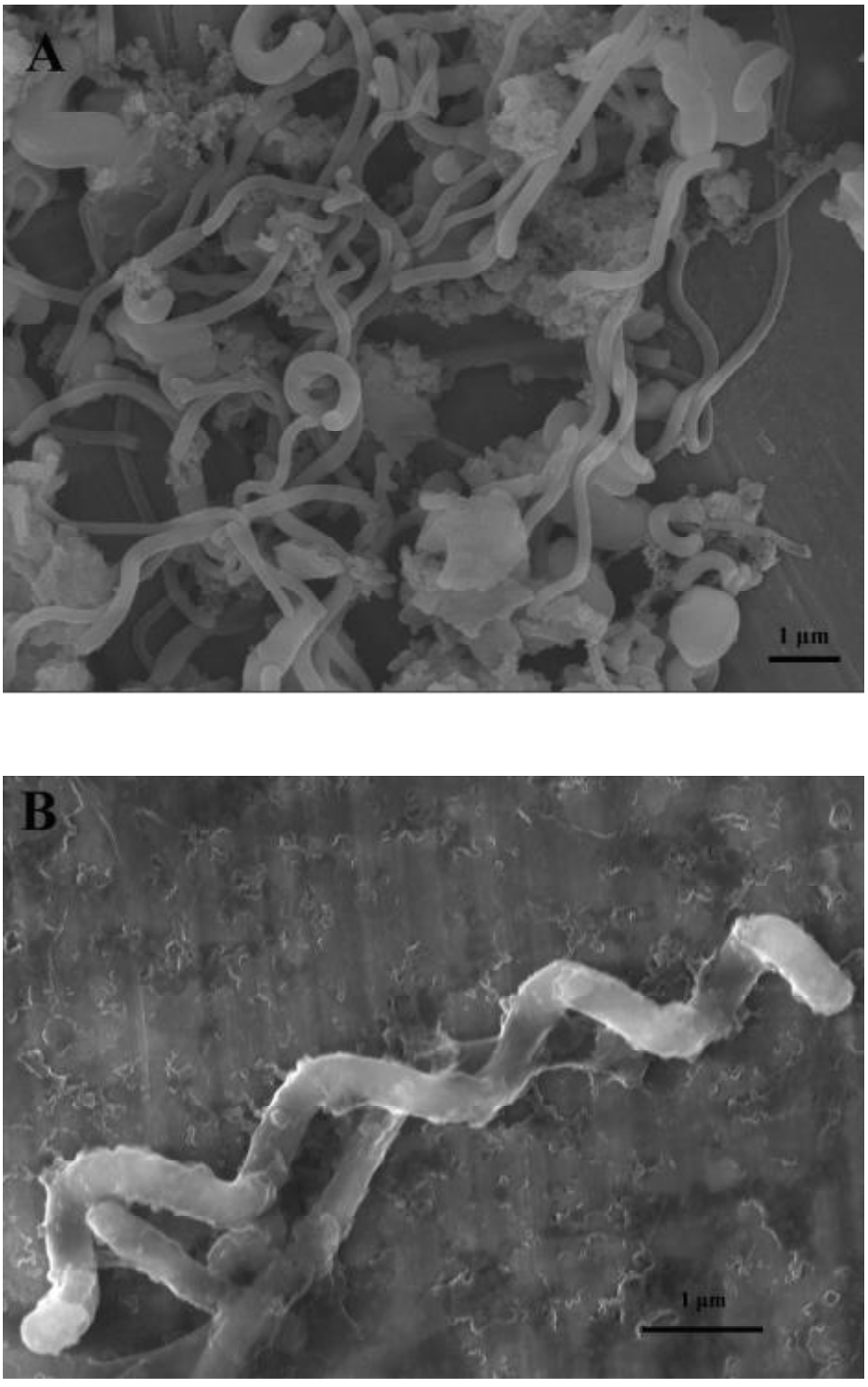

Figure 3.10 SEM images of helical MCM-41.

It has been found that the distributions of these anionic silicate species are sensitive to pH, temperature, cation, and Si concentration. A reduction in silicon concentration or increase in temperature or pH favors the formation of monomer and small oligomers [64]. One of the reasons of choosing dilute solution is because increasing silicate concentration results in the large extent of oligomerization.

As described previously, the phase organization of surfactant and inorganic polymerization are the two main processes during the formation of mesoporous silica. Fast inorganic condensation will be a serious problem for morphology control. From the kinetic point of view, in conditions where condensation is slow, the kinetic constants of the different processes should be ordered as follows:

$$k_{inter} > k_{org} > k_{inorg} \tag{3.4}$$

We used the extremely dilute solution routes to investigate the effects of temperature, stirring speed and seed crystal, which are directly affecting the interactions to generate a well-defined hybrid interface. Under the dilute solution condition, these experiment parameters can provide an effective way to control gelation and precipitation processes, and subsequently control the morphologies of MCM-41 silica.

CHAPTER 4 ENCAPSULATION OF GEMANIUM NANOPARTICLES INSIDE MCM-41 MESOPORES

Recent success in growing and loading semiconductors like Si [65], TiO_2 [66], GaAs [67], CdS [68, 69] into the MCM-41 mesopores has opened a new research field in the electronic and optical applications of mesoporous silica. Due to the quantum confinement effects and guest-host effects, the semiconductor/mesoporous composites exhibit unique optical properties, such as blue-shift, fluorescence, photoluminescence. Compare with Si, Ge is an important VI semiconductor with a narrow bandgap and similar electron affinity [70].

In this study, we chose $GeBr_4$ or GeH_4 as the metal ion sources, in contrast to the traditional starting materials such as the expensive and toxic $GeCl_2$·dioxane used in previously reported synthesis route [71, 72]. We also developed three different synthesis methods to compare the pore filling efficiency of Ge semiconductors in the silica networks.

4.1. H_2 reduction method

4.1.1. Experiment method

In this synthesis, $GeBr_4$ was used as Ge precursor and the formation of Ge nanoparticles was completed by H_2 reduction. Three samples were obtained under different experiment condition. Sample 1 was the result of single impregnation of the precursor and sample 2 was obtained after multiple impregnations. Sample 3 was the products of multiple impregnations and was annealed at 823 K.

The first step of our synthesis process concerns the homogeneous adsorption of Germanium cationic species on the silica walls that form the pore surface, which is completed by impregnation of the THF solutions with soluble Germanium cationic species. Figure 4.1 schematically shows the chemical process of this step. Because the silica walls are partially soluble when the pH is above 10 [73], THF solutions were used here instead of aqueous solutions.

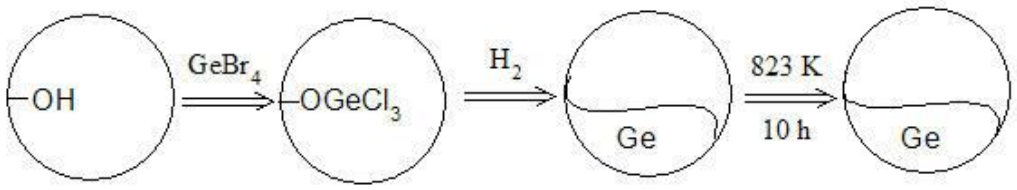

Figure 4.1 schematic reaction sequences for the synthesis of Ge nanoparticles in MCM-41.

The impregnated MCM-41 powders were washed by THF solutions, EtOH and distilled water to eliminate reactive in excess, and above all to avoid the accumulation of cationic species at the outer surface of MCM-41 powders.

The last step of the process is the homogeneous formation of nanoparticles via the precipitation of the ionic species. This requires the use of gaseous hydrogen, which rapidly diffuses into the film leading to simultaneous precipitation within all the pores.

4.1.2. Electron Microscope results

The TEM image of Ge@MCM-41 composite from single impregnation is shown in Figure 4.2. It reveals that the hexagonally ordered mesostructure (Figure 4.2B, higher magnification) of the host material MCM-41 was unaffected by the presence of Ge inside the pores. This indicates that the H_2 reduction technique does not cause significant deterioration of MCM-41 framework. The Ge@MCM-41 composite exhibits two basic types of diffraction pattern. The electron diffraction patterns shown in Figure 4.2C are obtained by viewing the Ge@MCM-41 composite along the axis of the hexagonal pores. This gives a [0001] pattern with six-fold symmetry. When viewed normal to the hexagonal pore axis, a one-dimensional diffraction pattern was obtained (Figure 4.2D) These electron diffraction patterns are in good agreement with the reported results [74] and confirm that the ordered network of MCM-41 material was unaffected by the growth of Ge particles inside the pores of MCM-41.

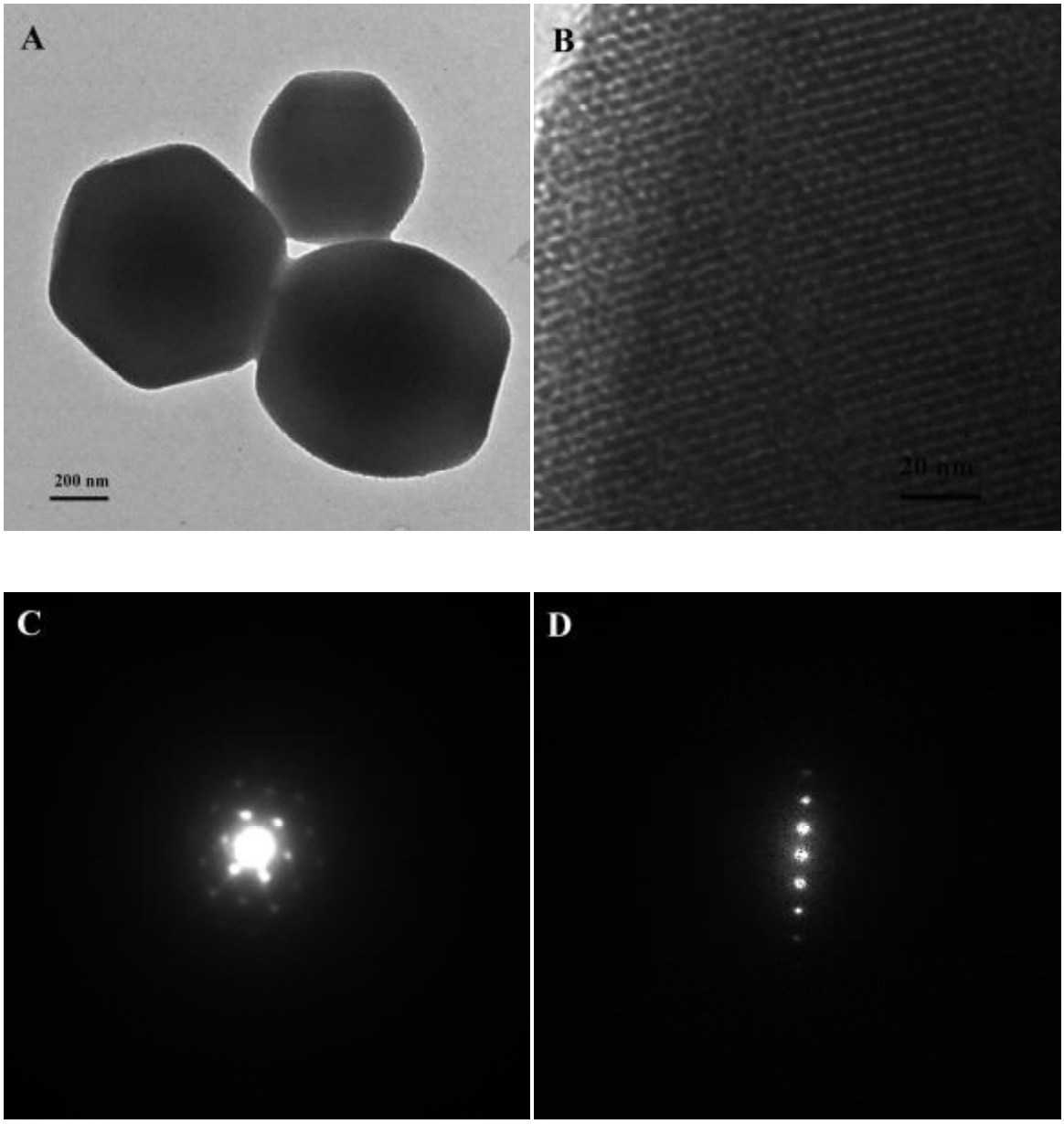

Figure 4.2 TEM images of Ge@MCM-41 sample 1: A) TEM image of Ge@MCM-41 composite particles. B) High magnification of a single Ge@MCM-41 particle. C) Electron diffraction pattern of Ge@MCM-41 composite particle viewing along the axis of hexagonal pores. D) One-dimensional electron diffraction pattern of Ge@MCM-41 obtained by viewing normal to the hexagonal pore axis.

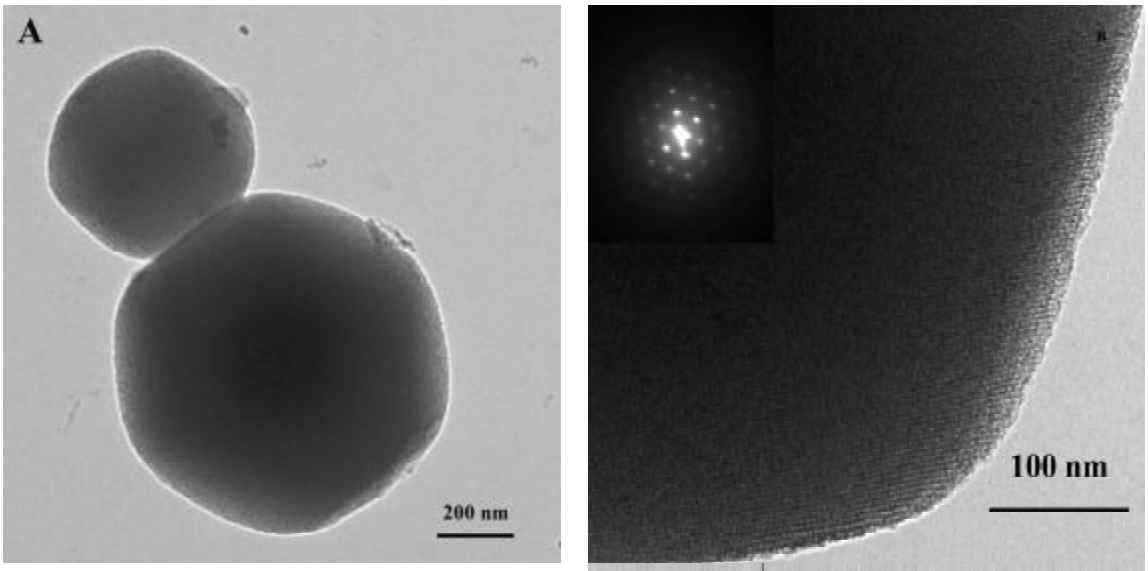

Figure 4.3 TEM images of Ge@MCM-41 sample 2. A) Scale bar, 200 nm. B) Scale bar, 100 nm.

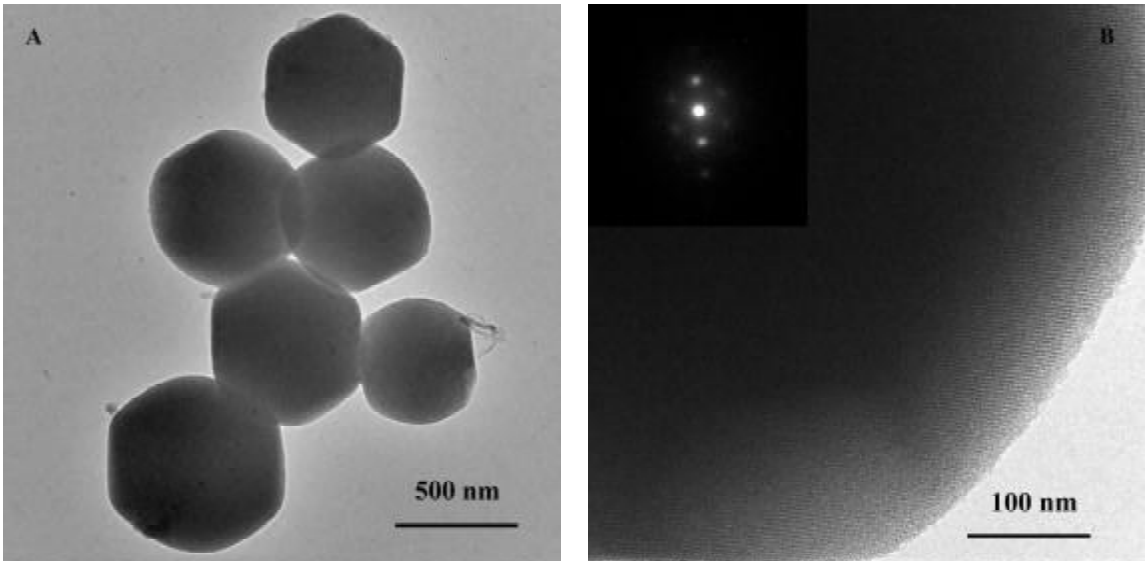

Figure 4.4 TEM images of Ge@MCM-41 sample 3: A) Scale bar, 500 nm. B) Scale bar, 100 nm.

The Ge nanoparticles inside the channels of MCM-41 are also confirmed by high magnification TEM images shown in Figure 4.2B, Figure 4.3B and Figure 4.4B. The Ge nanocrystallites appear as dark substances among the channels of MCM-41. The diameter of these nanocrystallites is about 3 nm due to the limitation of MCM-41 nanochannels.

The TEM analysis (Figure 4.4) and SEM results (Figure 4.5) of sample 3 showed the thermal stability of MCM-41 mesostructures after annealing at 823 K. In addition, Ge@MCM-41 composite exhibits stronger electron contrast than the empty MCM-41 and moreover the semiconductor-filled composite was much more stable under the electron beam than the empty MCM-41 (Figure 3.2D). These observations indicate that the inner walls of the silica host material have been coated with Ge particles.

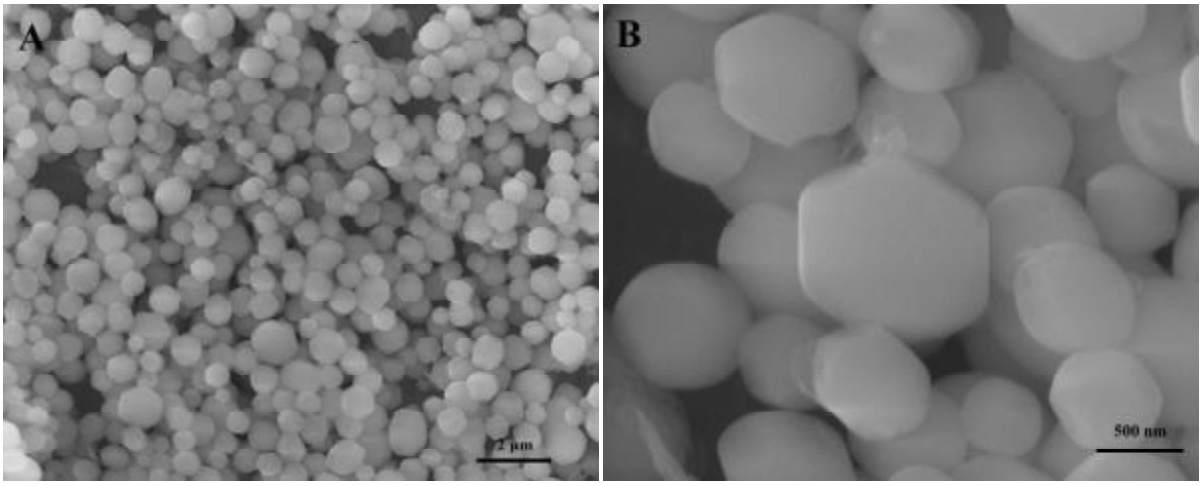

Figure 4.5 SEM images of sample 3: A) Scale bar, 2 um. B) Scale bar, 500 nm.

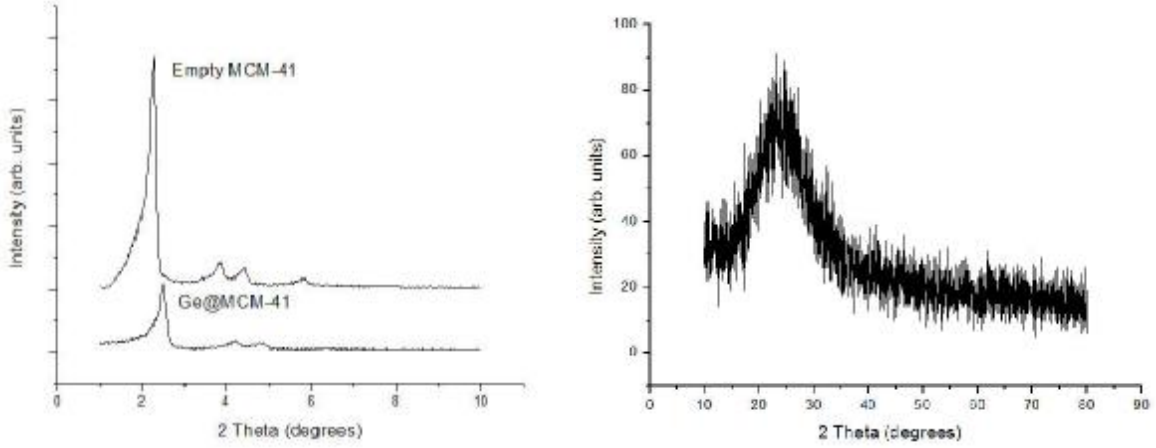

Figure 4.6 A) Low-angle (2θ=1-10^{o}) XRD pattern of empty MCM-41 and loaded Ge@MCM-41. B) Wide-angle (2θ=10-80^{o}) XRD pattern of loaded Ge@MCM-41.

4.1.3. XRD results

The calcined MCM-41 was vacuum dried and characterized by low-angle XRD measurements, which exhibit the characteristic reflections of high-quality hexagonal mesostructures (Figure 4.6).

Figure 4.6A shows the comparison of XRD patterns of empty MCM-41 and Ge@MCM-41 composites for the low-angle region (2θ=1-10^o). It is observed that the highly ordered hexagonal pore structure of MCM-41 is still intact, while the intensities of the characteristic XRD reflections of MCM-41 are reduced for Ge@MCM-41. This can be attributed to pore filling of the host material, which reduces the scattering contrast between the pores and the walls of the molecular sieve [75] (particles are confined to the pores of MCM-41).

In addition, the peaks of Ge@MCM-41 sample are obviously shifted to higher angle. The pore size estimated from the equation (d_{100} – 1) nm is reduced from 2.6 nm to 2.0 nm. This also provides evidence for the pore filling of Ge nanoparticles.

Figure 4.6B shows the wide-angle XRD pattern of Ge@MCM-41. A very broad reflection peak at 26^o corresponds to the diffraction of the amorphous wall of MCM-41. There is no direct evidence in the XRD pattern showing the crystallinity of Ge nanoparticles inside MCM-41. We suggest the XRD peaks of Ge crystal may be too weak and too broad to be observed due to the small size of the nanoparticle (< 2.6 nm).

4.1.4. EDS analysis

To confirm the formation of Ge nanoparticles, three samples were characterized by EDS (Figure 4.7). The EDS analysis was performed on the mesoporous region (where no Ge particles are externally visible). Figure 4.7B shows stronger Ge signals than Figure 4.7A indicating the confinement of Ge nanoparticles inside the pores of MCM-41 was enhanced by multiple precursor impregnations. In the EDS analysis, in addition to Ge peaks, Si and O peaks (MCM-41) as well as Cu and C peaks (support grid) and Br (surfactants) were detected. From the EDS spectrum an approximate ratio of 1.6:0.4 for Si:Ge, and 1.6:1.5 for Si:O was calculated.

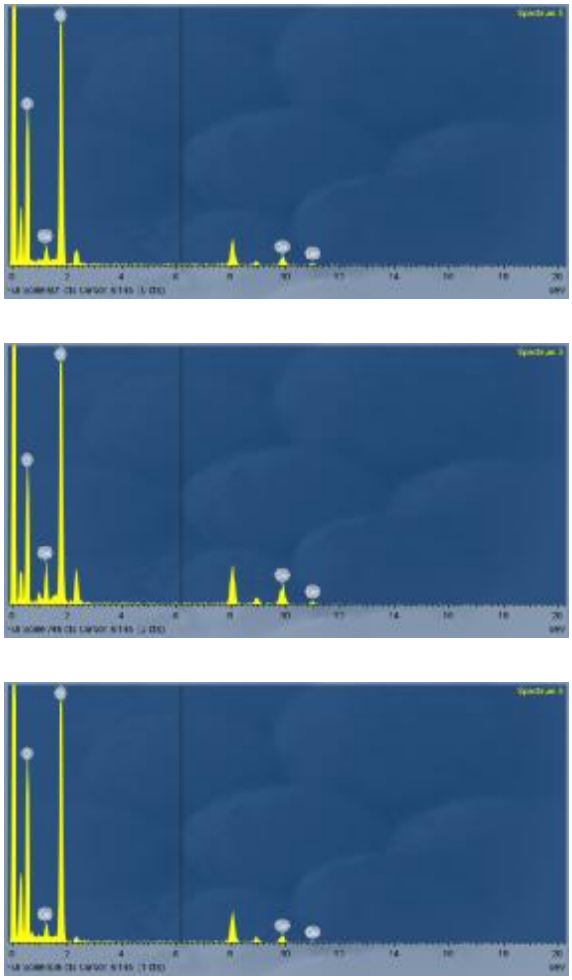

Element	Weight%	Atomic%
O K	31.35	47.81
Si K	54.65	47.48
Ge K	14.00	4.71
Totals	100.00	

Element	Weight%	Atomic%
O K	23.57	41.86
Si K	45.54	46.06
Ge K	30.89	12.09
Totals	100.00	

Element	Weight%	Atomic%
O K	37.06	54.03
Si K	50.56	41.99
Ge K	12.38	3.98
Totals	100.00	

Figure 4.7 EDS patterns of three samples through H_2 reduction synthesis route: A) Sample 1 via single impregnation. B) Sample 2 via multiple impregnations. C) Sample 3 via multiple impregnations and after calcinations.

4.1.5. N_2 adsorption-desorption study

Figure 4.8 shows the nitrogen adsorption-desorption isotherms of empty MCM-41 powder and Ge@MCM-41 powder. The results were obtained at 77 K. All of the isotherms are of type IV classification, which is typical adsorption of mesoporous materials [76].

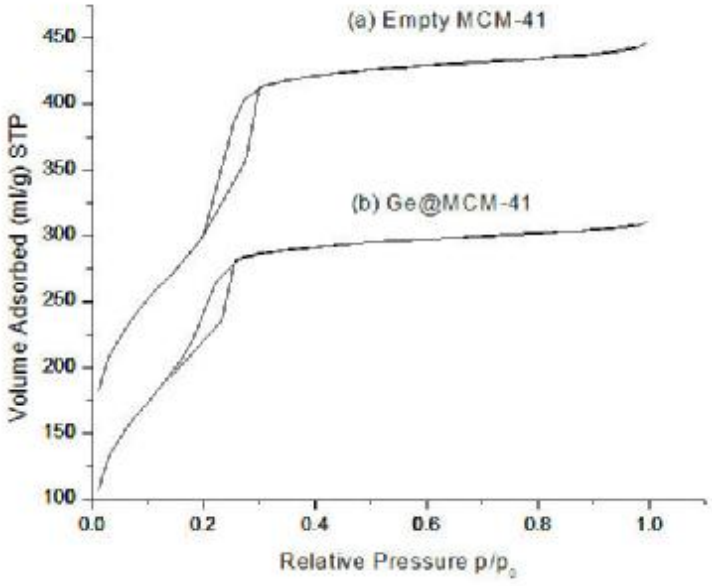

Figure 4.8 Nitrogen adsorption-desorption isotherms of (a) Empty MCM-41 and (b) Ge@MCM-41.

The BET surface area of the empty MCM-41 was 922 m^2/g and the pore-size distribution of about 2.7 nm (full-width at half-maximum, FWHM = 0.2 nm) was calculated from BJH (Barrett-Joyner-Halender) theory [77] on the basis of desorption data from the N_2 studies. The pore size was estimated as the value corresponding to the maximum of the BJH pore-size distribution.

The N_2 sorption studies on Ge@MCM-41 proved evidence of pore filling of the host matrix. A well-defined step occurs approximately at p/p_0 = 0.1 ~ 0.3, which is associated with the filling of the mesopores due to capillary condensation. After formation of nanoparticles, the amount of adsorbed nitrogen decreases and the inflection point of the step shifts to a smaller p/p_0. This is directly showed as decrease in pore volume of Ge@MCM-41 with respect to empty MCM-41. The decrease in BET surface area of Ge@MCM-41 (713 m^2/g) in comparison with that of empty MCM-41 (922 m^2/g), also implies Ge semiconductor clusters have been confined inside the channels of MCM-41.

Loading Ge nanoparticles into MCM-41 through H_2 reduction is actually a process of in situ formation of the Ge nanoparticles inside mesoporous MCM-41. The hydroxyl group on the internal surface of MCM-41 will easily absorb the $GeBr_4$ molecules to form Si-O- $GeBr_3$ species (Figure 4.1). The gaseous hydrogen diffuses quickly in the pore systems and reduces the Ge^{4+} ions to form Ge nanoparticles. The reaction can be described as follows:

$$MCM41 + GeBr_4 \rightarrow MCM41 - GeBr_3 + HBr \quad (4.1)$$

$$MCM41 - GeBr_3 + \tfrac{3}{2}H_2 \rightarrow Ge@MCM41 + 3HBr \quad (4.2)$$

4.2. Vapor phase epitaxy

4.2.1. Experiment method

In this synthesis route, Germane (GeH_4) was used as Ge precursor. The host MCM-41 was vacuum dried for 4 h to remove the surfactant and organic species inside the pore system. Then the vapor phase GeH_4 was introduced into the mesopores of MCM-41 under constant flow for continuous 1 h. After the gaseous GeH_4 was homogeneously dispersed in the pore system, the reaction chamber was heated up to 823 k leading to the pyrolysis of the precursors.

4.2.2. Results and analysis

Figure 4.10 shows the representative TEM images for the Ge@MCM-41 synthesized through this method. The high magnification TEM image (Figure 4.10B) revealed that the mesoporous structures are intact after loading Ge nanoparticles inside the pores. However, the dark edge and some dark spots with diameters ranging from 5 to 15 nm show that a great amount of Ge grew on the outside surface of the host MCM-41. From the ratio of dark spots and white spots in the HRTEM image it can be estimated that only half of the pores were successfully loaded with Ge nanoparticles, which may be attributed to the low yield of gaseous precursor. Although the gas flow in the reaction chamber was continuous, it may not flow into the pore system consecutively. On the other hand, the host MCM-41 was immersed in the gas phase and once the pyrolysis process was triggered, most of the pryolysis products (Ge) would precipitate on the outside surface of the host MCM-41 and prevent more gaseous precursor getting inside the pore system.

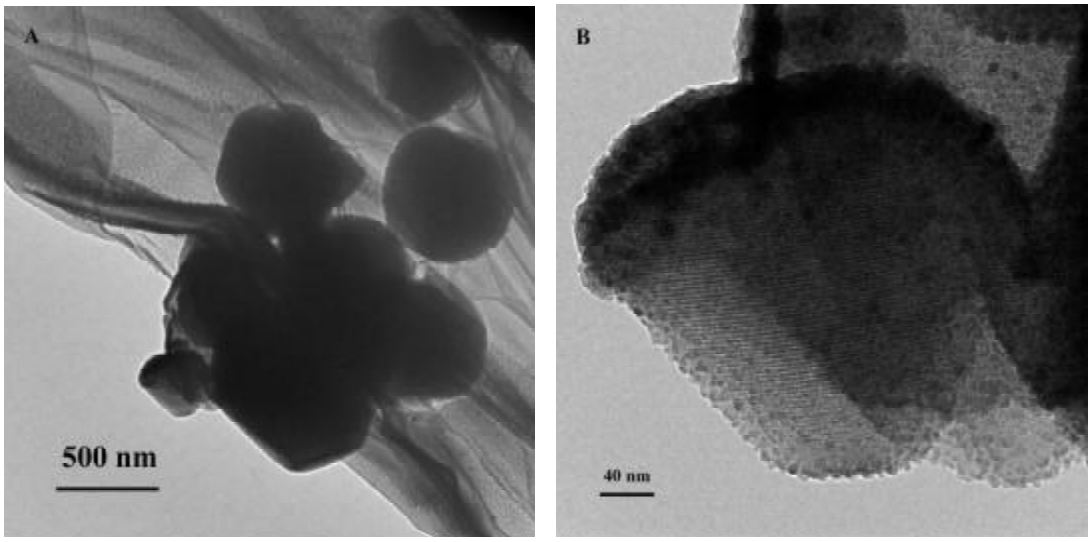

Figure 4.9 TEM images of Ge@MCM-41 synthesize through Vapor phase epitaxy method.

4.3. Redox reaction using Na-Naphthalene

4.3.1. Experiment method

The Ge nanoparticles were introduced within the mesoporous powders by impregnation with a THF solution of $GeBr_4$ and followed by a reduction reaction through Na-Naphthalene solution.

A chemical attachment of a molecular precursor for germanium was obtained by reacting neat $GeBr_4$ with the silanol groups at the surface of the mesoporous ordered MCM-41 at room temperature. The excess of $GeBr_4$ was removed in vacuo and the functionalized MCM-41 was vacuum dried for several hours in order to remove residual hydrogenbromide. Subsequently, an excess of a 1M solution of Na-Naphthalene in THF was added to produce an orange-colored, X-ray amorphous hydrogenated germanium in the pores of the substrate. Annealing of this material at 773 K for 2 h (under argon atmosphere) yielded grey crystalline germanium in the mesopores of MCM-41.

4.3.2. Results and analysis

To confirm the formation of Ge nanoparticles, the sample was characterized by EDS (Figure 4.11). A very strong signal of Ge was shown in the EDS pattern, which suggests the successful loading the Ge semiconductor clusters in the mesoporous structures.

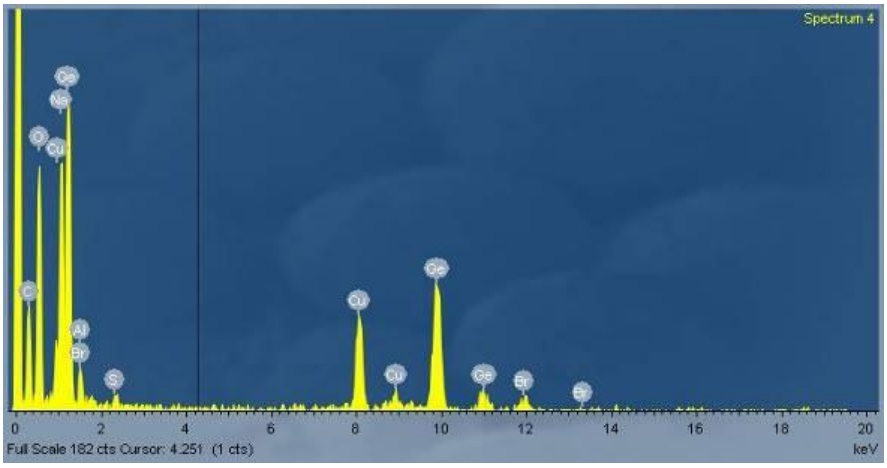

Figure 4.10 EDS pattern of Ge@MCM-41 composites synthesized through Na-Naphthalene reduction.

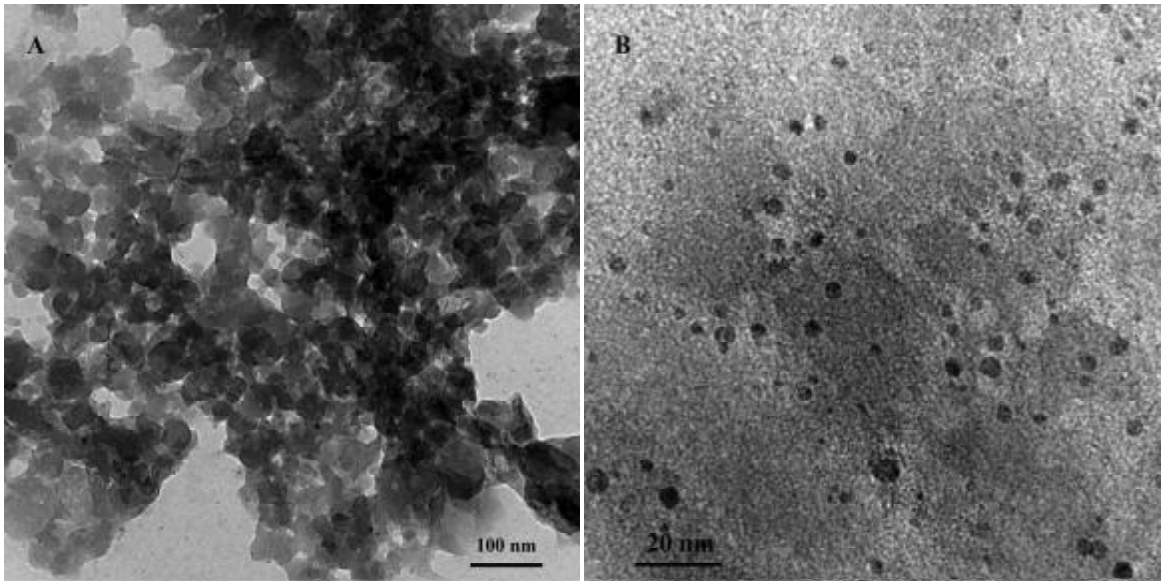

Figure 4.11 TEM images of Ge@MCM-41 synthesized through Na-Naphthalene reduction.

The TEM results of Ge@MCM-41 show that most of the silica networks have been destroyed and many Ge nanoparticles with size bigger than the host MCM-41 pore size (2.6 nm) have been observed (Figure 4.12).

4.4. Summary

Three different synthesis methods have been used to grow monodisperse Ge nanoparticles in the mesoporous silica networks.

The H_2 reduction synthesis route to incorporate Ge nanoparticles into 3D hexagonal mesoporous silica is very simple and effective and can be generalized to other II-VI semiconductors. X-ray diffraction and electron microscopy characterizations unambiguously demonstrate that the mesoporous structure allows to control the particle size and the organization of Ge nanoparticles. This leads to the growth of a 3D lattice of semiconductors at a large scale. The impregnation of precursor solutions can be well controlled because the hydroxyl functional groups bind with $GeBr_4$ easily and this step can be repeated many times until the full filling of the pores of MCM-41. The gaseous H_2 can penetrate the pore system quickly to reduce Ge^{4+} to Ge.

The vapor phase epitaxy method can also successfully load Ge into the pore system. For full filling Ge nanoparticles of the pores of MCM-41, multiple cycles of outside surface washing-vapor phase epitaxy seems to be feasible. However the expensive precursors limit the broad use of this method.

The breakage of the mesostructures of MCM-41 caused by Na-Naphthalene solution suggests the importance of choosing proper solvent. The interaction between the pore walls and solvent directly affects the delivery of precursors.

CHAPTER 5 CONCLUSIONS

Highly ordered hexagonal arrayed mesoporous silica host MCM-41 were successfully synthesized through an extremely dilute solution route of surfactant and silicate. Based on the surfactant templating theories, we studied the crucial experimental parameters of this synthesis approach and found that a slow growing rate is the fundamental requirement for the morphology control of mesostructured MCM-41 silica. Several kinds of mesostructured silica with characteristic-shaped morphologies were achieved, such as spheres, films, rods, rice-like particles and helical MCM-41.

From the electron microscope results, the spherical MCM-41 particles are monodisperse and have a uniform size of ~ 500 nm. The mesopores of MCM-41 silica are highly ordered and exhibit very high thermal stability after annealing at 823 K. The XRD results of the sample also show the well ordered periodic structures of MCM-41 particles before and after annealing. Nitrogen sorption results show that the BET surface area of MCM-41 particles is 922 m^2/g. The average diameter of the mesopores is about 2.7 nm, which is an ideal size for applying quantum confinement effect on the particles inside the channels. Thus MCM-41 spheres are promising host materials for incorporating semiconductor nanoparticles.

We used the prepared MCM-41 spheres as host materials and successfully loaded Ge nanoparticles inside the channels of MCM-41 through three different routes. The vapor phase epitaxy method is a simple way for loading Ge nanoparticles into MCM-41 mesopores using GeH_4 as the precursor followed by pyrolysis. However such method requires pure gas phase and the efficiency of loading is low, which may be improved by multiple cycles of growth. A viable technique is the combination of a wet impregnation technique and the reduction of loaded organometallic precursors. We found that during the reduction process, the interaction between the pore walls of MCM-41 and synthesis solution plays an important role in preserving the pore structures. Using H_2 as the reducing agent not only avoids this problem, but also has many other advantages such as homogenous distribution, simultaneous reaction and free of residues.

The characterization results of the samples showed that the H_2 reduction method is a simple and cost effective fabrication technique for the assembly of Ge nanoparticles into MCM-41 networks. The as-prepared Ge@MCM-41 composites may have applications in optic field and

electronic field. Future investigations may focus on the quality control (particle size, crystallinity, polydispersity, etc) of the Ge nanoparticles inside the pores of MCM-41 during the process of encapsulation.

REFERENCES

[1] Sing, K. S.; Everett, D. H. and Haul, R. A. W. *Pure Appl. Chem.*, **1972**, *31*, 578.

[2] Soler-Illia, G. J.; Sanchez, C.; Lebeau, B., et al. *Chem. Rev.*, **2002**, *102*, 4093.

[3] Avelino, C. *Chem. Rev.* **1997**, *97*, 2373.

[4] Vallet-Regi, M.; Ramila, A.; del Real, R. P., et al. *Chem. Mater.* **2001**, *13*, 308.

[5] Imhof, A. and Pine, D. J. *Nature* **1997**, *389*, 948.

[6] Wijnhoven, J. E. G. J. and Vos, W. L. *Science* **1998**, *281*, 802.

[7] Beck, J. S.; Vartuli, J. C.; Roth, W. J., et al. *J. Am. Chem. Soc.* **1992**, *114*, 10834.

[8] Kresge, C. T.; Leonowicz, M. E.; Roth, W. J., et al. *Nature* **1992**, *359*, 710.

[9] Inagaki, S.; Fukushima, Y.; Kuroda, K. *J. Colloid Interface Sci.*, **1996**, *180*, 623.

[10] Lukens, W. W.; Schmidt-Winkel, P.; Zhao, D.; Feng, J.; Stucky, G. D. *Langmuir*, **1999**, *15*, 5403.

[11] Bagshaw, S. A.; Prouzet, E.; Pinnavaia, T. J. *Science*, **1995**, *269*, 1242.

[12] Luan, Z.; Zhao, D.; He, H.; Klinowski J.; Kevan, L. *J. Phys. Chem. B*, **1998**, *102*, 1250.

[13] Ryoo, R.; Joo, S. H.; Jun, S. *J. Phys. Chem. B*, **1999**, *103*, 7743.

[14] Raman, N. K., Anderson, M. T. and Brinker, C. J. *Chem. Mater.*, **1996**, *8*, 1682.

[15] Vartuli, J. C.; Schmitt, K. D.; Kresge, C. T., et al. *Chem. Mater.* **1994**, *6*, 2317.

[16] Vartuli, J. C.; Kresge, C. T.; Leonowicz, M. E., et al. *Chem. Mater.* **1994**, *6*, 2070.

[17] Chen, C. Y.; Li, H. Y.; Davis, M. E. *Microporous Mater.* **1993b**, *2*, 27.

[18] Firouzi, A.; Kumar, D.; Bull, L. M., et al. *Science* **1995**, *267*, 1138.

[19] Huo, Q.; Margolese, D. I.; Ciesa, U., et al. *Chem. Mater.* **1994**, *6*, 1176.

[20] Soler-Illia, G. J.; Crepaldi, E. L.; Grosso, D., et al. *Curr. Opin. Colloid Interf. Sci.* **2003**, *8*, 109.

[21] Soler-Illia, G. J.; Scolan, E.; Louis, A., et al. *New J. Chem.* **2001**, *25*, 156.

[22] Soler-Illia, G. J. and Sanchez, C. *New J. Chem.* **2000**, *24*, 493.

[23] Brinker, C. J.; Scherer, G. W. Sol-gel Science: the Physics and Chemistry of Sol-Gel Processing. *San Diego: Academic Press*, **1990**

[24] Livage, J.; Henry, M. and Sanchez, C. *Prog. Solid State Chem.* **1988**, *18*, 259.

[25] Dislich, H. *Angew. Chem. Int. Ed.* **1971**, *10*, 363.

[26] Mackenzie, J. D. *J. Non. Cryst. Solids* **1985**, *73*, 631.

[27] Cheng, W. Synthesis and characterization of mesoporous materials. *In a doctorial dissertation of UCLA*, **2002**.

[28] Winter, G. J. *Oil and Colour Chemist's Association* **1953**, *34*, 30.

[29] Bistan, E. and Gomory, I. *Chem. Zvesti*, **1956**, *10*, 91.

[30] Klemperer, W. G.; Mainz, V. V.; Ramamurthi, S. D.; Rosenberg. "Better Ceramics Through Chemistry III", Brinker, C. J.; Clark, D. E.; Ulrich, D. R. Editors. *Materials Research Society: Pittsburgh, PA*, **1998**.

[31] Froba, M.; Kohn, R.; Bouffaud, G.; Richard, O. and Tendeloo, G. V. *Chem. Mater.*, **1999**,

11, 2858.
[32] Aggr, J. A.; Anderson, M. W.; Pemble, M. E.; Terasaki O. and Nozue, Y. *J. Phys. Chem. B*, **1998**, *102*, 3345.
[33] Srdanov, V. I.; Alxneit, I.; Stucky, G. D.; Reaves C. M. and Denbaars, S. P. *J. Phys. Chem. B*, **1998**, *102*, 3341.
[34] Stucky G. D. and MacDougall, J. E. *Science*, **1990**, *247*, 669.
[35] Leon, R.; Margolese, D. G.; Stucky G. D. and Petroff, P. M. *Phys. Rev. B*, **1995**, *52*, R2285.
[36] Chakraborty, P. *J. Mater. Sci.*, **1998**, *33*, 2235.
[37] Yang, P.; Wirnsberger, G.; Huang, H. C.; Cordero, S. R.; McGehee, M. D.; Scott, B.; Deng, T.; Whitesides, G. M.; Chmelka, B. F.; Buratto S. K. and Stucky, G. D. *Science*, **2000**, *287*, 465.
[38] Junges, U.; Jacobs, W.; Voigt-Martin, I.; Krutzsch, B.; Schuth,F. *J. Chem. Soc., Chem. Commun*. **1995**, 2283.
[39] Hartmann, M.; Poppl, A.; Kevan, L. *J. Phys. Chem*. **1996**, *100*, 9906.
[40] Schnider, M.; Wildberger, M.; Maciejeswski, M.; Duff, D. G.; Mallat, T.; Baiker, A. *J. Catal*. **1994**, *148*, 625.
[41] Zhang, Z. T.; Dai, S.; Hunt, R. D.; Wei, Y.; Qiu, S. L. *Adv. Mater*., **2001**, *13*, 493.
[42] Eddy, C. R. and Moustakas, T. D. *J. Appl. Phys.*, **1993,** *73*, 448.
[43] Miehr, A.; Ambacher, O. and Rieger, W. *Chem. Vapor Deposit*, **1996**, *2*, 5.
[44] Winkler, H.; Birkner, A.; Hagen, V.; Wolf, I.; Schmechel, R.; von Seggern, H. and Fischer, R. A. *Adv. Mater.*, **1999**, *11*, 1444.
[45] Khushalani, D.; Kuperman, A.; **Ozin**, G. A.; Tanaka, K.; Garcés, J.; Olken, M. M.; Coombs. N. *Adv. Mater.*, **1995**, *7*, 842.
[46] Huo Q.; Feng, J.; Schüth, F.; Stucky, G. D. *Chem. Mater*. **1997**, *9*, 14.
[47] Grün, M.; Lauer, I. and Unger, K. K. *Adv. Mater.*, **1997**, *9*, 254.
[48] Stöber, W.; Fink, A. and Bohn, E. *J. Colloid Interface Sci.*, **1968**, *26*, 62.
[49] Büchel. G.; Unger, K. K.; Matsumoto, A.and Tsutsumi, K. *Adv. Mater.*, **1998**, *10*, 1036.
[50] Unger, K. K.; Giesche, H.and Kinkel, J. N. *Chem. Abstr.*, **1987**, *106*, 179029y.
[51] Kaiser, C. and Unger, K. K. *German Patent DE-195 30031 A1*, **1997**.
[52] Inagaki, S.; Guan, S.; Ohsuna, T. and Teraski, O. *Nature*, **2002**, *416*, 204.
[53] Cai, Q.; Luo, Z. S.; Pang, W. Q., et al. *Chem. Mater*, **2001**, *13*, 258.
[54] Lin, H. P.; Mou, C. Y. *Science*, **1998**, *282*, 1302.
[55] Steel, A.; Carr, S. W.; Anderson, M. W. *J. Chem. Soc., Chem. Commun*., **1994**, 1571.
[56] Yano, K; Fukushima, Y. *J. Mater. Chem.*, **2004**, *14*, 1579.
[57] Boissiere, C.; Kummel, M.; Persin, M.; Larbor A. and Prouzet, E. *Adv. Funct. Mater.*, **2001**, *11*, 129.
[58] Gallis, K. W.; Araujo, J. T.; Duff, K. J.; Moore, J. G. and Landry, C. C. *Adv. Mater.*, **1999**, *11*, 129.
[59] Kurganov, A.; Unger, K. K. and Issaeva, T. *J. Chromatogr. A*, **1996**, *753*, *177*.
[60] Nassivera, T.; Eklund, A. G. and Landry, C. C. *J. Chromatogr. A*, **2002**, *973*, *97*.
[61] Lee, M-H.; Oh, S-G.; Moon, S-K. and Bae, S-Y. *J. Colloid Interface Sci.*, **2001**, *83*, 240.
[62] Patterson, L. K.; Vieil, E. *J. Phys. Chem.* **1973**, *77*, 1191.
[63] Yang, H.; Coombs, N.; Sokolov, I., et al. *Nature*, **1996**, *381*, 589.
[64] Kinrade, S. D. and Swaddle, T.W. *Inorg. Chem.*, **1988**, *27*, 4253.
[65] Chomski, E.; Dag, O.; Kuperman, A.; Coombs, N. and Ozin, G. A. *Chem. Vapor. Deposit.* **1996**, *2*, 8.

[66] Aronson, B. J.; Blanford, C. F. and Stein, A. *Chem. Mater.* **1997**, *9*, 2842.
[67] Srdanov, V. I.; Alxneit, I.; Stucky, G. D.; Reaves, C. M. and DenBaars, S. P. *J. Phys. Chem. B*, **1998**, *102*, 3341.
[68] Hirai, T.; Okubo, H. and Komasawa, I. *J. Phys. Chem. B*, **1999**, *103*, 4228.
[69] Zhang, Z.; Dai, S.; Fan, X.; Blom, D. A.; Pennycook, S. J. and Wei, Y. *J. Phys. Chem. B*, **2001**, *105*, 6755.
[70] Shi, Y.; Saito, K.; Ishikuro H. and Hiramoto, T. *Jpn. J. Appl. Phys.*, **1999**, *38*, 425.
[71] Mathur, S.; Shen, H.; Sivakov, V. and Werner, U. *Chem. Mater.* **2004**, *16*, 2449.
[72] Schlecht, S.; Himmel, H. J.; *Anorg. Allg. Chem.* **2003**, *629*, 2521.
[73] Iler, R. K. "In The Chemistry of Silica", **1979.**
[74] Leon R.; Margolese, D.; Stucky G., et al. *J. Phys. Chem. B*, **1995**, *52*, R2285.
[75] Marler, B.; Oberhagemann, U.; Vortmann, S.; Gies, H. *Microporous Mater.* **1996**, *6*, 375.
[76] Sheng, S. *J. Mater. Chem.*, **2001**, *11*, 578.
[77] Barrett, E. P.; Joyner, L. G. and Halenda, P. P. *J. Am. Chem. Soc.* **1951**, *73*, 373.

VITA

The author was born in Sichuan, China in 1979. He began his undergraduate study in the Department of Materials and Engineering at the University of Science and Technology of China in 1998. He obtained his B.S. degree in 2003. In 2004, he came to University of New Orleans and joined Professor Jiye Fang's research group to continue his graduate study in Materials Science.